Journal of Structural Geology 32 (2010) 667–684

Contents lists available at ScienceDirect

Journal of Structural Geology

journal homepage: www.elsevier.com/locate/jsg

Fault–slip analysis and transpressional tectonics: A study of Paleozoic structures in northern Victoria Land, Antarctica

L. Federico*, L. Crispini, G. Capponi

University of Genova, Dip.Te.Ris., Corso Europa 26, Genova, Italy

ARTICLE INFO

Article history:
Received 5 October 2009
Received in revised form
29 March 2010
Accepted 1 April 2010
Available online 7 April 2010

Keywords:
Fault–slip analysis
Transpressional tectonics
Northern Victoria Land
Antarctica

ABSTRACT

The brittle structures of the Bowers Mountains (northern Victoria Land, Antarctica) have been studied in order to fully characterise the poorly described pre-Cenozoic brittle tectonics of this area. Field work revealed that the dominant structures are steeply-dipping reverse and strike-slip faults, locally associated with positive flower structures, diffuse veining and hydrothermal alteration. Field observations are combined with different methods of inversion of fault–slip data and with use of different open-source computer programs, that calculate resolved stress tensors and *P–B–T* axes in order to unravel the complex polyphase brittle architecture.

The resolved regional stress field is characterized by *E–W* trending, horizontal σ_1 and local rotations into NE–SW directions in the Lanterman Range/Sledgers Glacier area, due to subsequent block rotation or to the interference between the far-field stress with pre-existing ductile discontinuities.

The paleostress regime, unique overall structural framework and association with hydrothermal veining together with the strong similarities to deformation related to the Benambran Orogeny in the Lachlan fold belt in SE Australia supports the occurrence of a Late Ordovician–Silurian deformational event in northern Victoria Land (Antarctica).

1. Introduction

Antarctica presents many challenges to structural geologists due to its remote location and, in many areas, relatively poor exposure. Rocks now exposed in northern Victoria Land were part of the over 4000 km long paleo-Pacific margin of East Gondwana during the Paleozoic. This margin was the site of protracted convergence, with terrane accretion and collision(s) of arc and/or microcontinental masses (e.g., Veevers, 2000; Cawood, 2005; Vaughan and Pankhurst, 2008). The Ross–Delamerian (hereafter Ross) Orogeny (Cambrian–Early Ordovician; e.g., Bradshaw, 1987, 1989; Kleinschmidt and Tessensohn, 1987; Findlay et al., 1991; Ferraccioli et al., 2002) was the most pervasive tectonic event of the area, responsible for the regionally dominant deformations. Following that event, an outboard migration of the subduction plane possibly occurred inducing less intense deformations typical of foreland areas during the Devonian–Carboniferous, together with a magmatic pulse (Kleinschmidt and Tessensohn, 1987; Fioretti et al., 1997). Finally, the fragmentation of Gondwana and, in particular, the separation between Australia and Antarctica was responsible for strike-slip to transtensional deformations during the Cenozoic (e.g., Salvini et al., 1997; Rossetti et al., 2003). The area was, therefore, the site of multiple tectonic events, with recurrent reactivation of major faults, in particular the trans-lithospheric faults that represent terrane-bounding structures (e.g., Lanterman Fault and Leap Year Fault, Figs. 1, and 2).

The Cenozoic brittle tectonics of the northern Victoria Land has been widely documented in the published literature (Salvini et al., 1997; Salvini and Storti, 1999; Rossetti et al., 2000, 2002, 2003; Storti et al., 2001) whereas older brittle structures related to post-Ross orogenic phases are less well known (Wodzicki and Robert, 1986; Jordan et al., 1984; Capponi et al., 1999).

In this study we analyse and interpret the deformation patterns from outcrops located in an area that straddles the Lanterman and Leap Year faults focusing on the brittle structures related to pre-Cenozoic tectonics. A complex fault network is preserved, with dominant steeply-dipping reverse and oblique–slip faults, locally forming positive flower structures. The fault system is associated with quartz–carbonate veining and cuts and thus postdates the Ross Orogeny-related ductile deformation structures.

The aim of this work is to unravel the Paleozoic post-Ross Orogeny tectonic evolution, by characterising the tectonic event responsible for the development of the pre-Cenozoic fault system and related stress state. Regional correlations with the formerly adjoining fragments of Gondwana, namely SE Australia, are also discussed.

* Corresponding author.
E-mail address: federico@dipteris.unige.it (L. Federico).

0191-8141/$ – see front matter © 2010 Elsevier Ltd. All rights reserved.
doi:10.1016/j.jsg.2010.04.001

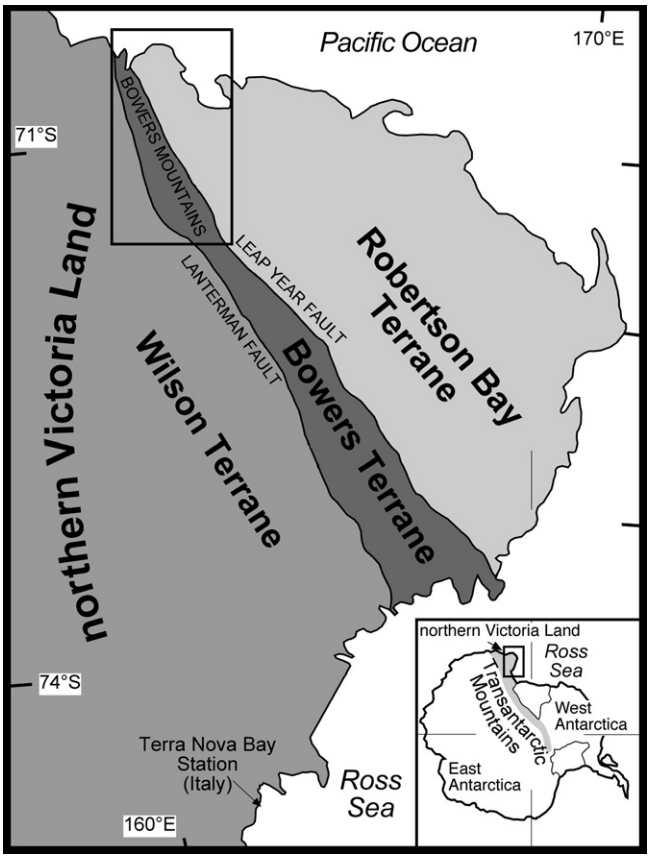

Fig. 1. Schematic geological map of northern Victoria Land with terrane boundaries and its location in the Antarctic continent. Squared area indicates the study area.

To achieve this aim, we conducted field work, investigating cross-cutting relationships, mesoscale fault geometries, and collecting fault–slip data. The inversion of fault–slip data is a well-established technique that has increasingly been used to unravel very complex tectonic histories, responsible for the formation of heterogeneous fault populations (e.g., Wang and Neubauer, 1998; Lamarche et al., 1999; Matenco and Schmid, 1999; Saintot and Angelier, 2002; Burg et al., 2005; De Paola et al., 2005; Bergerat et al., 2007; Laó-Dávila and Anderson, 2009; De Vicente et al., 2009; Sippel et al., 2009). Fault–slip inversion techniques have a number of critical assumptions and limitations (as discussed, for instance, by Pollard et al., 1993; Dupin et al., 1993; Twiss and Unruh, 1998; Marrett and Peacock, 1999), so we applied several different inversion methods and a variety of open-source computer programs to calculate resolved stress tensors (F.S.A. v. 28.5 by Célérier, 1999 and MIM 5.31 by Yamaji et al., 2005a) and *P–B–T* axes (Faultkin v. 4.3.5 by Allmendinger et al., 1994).

2. Geological and structural setting

2.1. Northern Victoria Land

The tectonic architecture of northern Victoria Land (Figs. 1 and 2) was predominantly established during the Neoproterozoic to early Paleozoic Ross Orogeny.

This event led to the accretion of three terranes to the East Antarctic craton: from west to east these are: the Wilson; Bowers; and Robertson Bay terranes (e.g., Bradshaw et al., 1985; Kleinschmidt and Tessensohn, 1987; Ricci et al., 1997; Federico et al., 2006). The Wilson and Bowers terranes are juxtaposed by the Lanterman Fault (e.g., Capponi et al., 1999), whereas the boundary between Bowers and Robertson Bay terranes is marked by the high-strain belt of the Millen Schist (Jordan et al., 1984; GANOVEX Team, 1987; Capponi et al., 2005).

The Wilson terrane represents the root of a Cambrian continental magmatic arc, with widespread granitoids of the Granite Harbour Igneous Complex intruding high- to low-grade metasedimentary country rocks (e.g., Borg and Stump, 1987). The Bowers terrane mainly consists of very low- to low-grade Cambrian metasedimentary (Molar Formation) and metavolcanic rocks (Glasgow Volcanics, Weaver et al., 1984; Laird, 1987) of arc/backarc affinity (Rocchi et al., 2003). The Robertson Bay terrane is formed by a thick succession of mainly very low-grade Cambro-Ordovician metaturbidites (Wright et al., 1984).

After docking during the Ross Orogeny, all three terranes were intruded by Devonian/Carboniferous calcalkaline intrusives (Admiralty Intrusives; Borg et al., 1984), associated with felsic volcanics (Gallipoli Volcanics). This magmatic suite is possibly linked to a poorly known orogenic event known as the Borchgrevink Orogeny (Grindley and Warren, 1964; Capponi et al., 2002).

The progressive erosion of the Ross Orogen down to its crystalline core produced a peneplain, with exhumation of 10–20 km in many places (Stump, 1995). This surface is overlain by the Beacon Supergroup, a Devonian to Triassic sedimentary sequence largely of terrestrial origin (Barrett, 1981; Collinson, 1991), followed by tholeiitic magmatism of Jurassic age (Ferrar Dolerite and Kirkpatrick Basalt). At present this cover sequence is visible only in the Wilson and Bowers terranes. Lastly, post-Jurassic tectonics, linked to the fragmentation of Gondwana and to the opening of the strongly asymmetric West Antarctic Rift System, is responsible for the present day high-elevation of the Transantarctic Mountains located on the asymmetric rift shoulder and for the reactivation of the inherited Paleozoic discontinuities (e.g., Salvini et al., 1997). Cenozoic transtensional tectonics is thought to have triggered the emplacement of alkaline volcanics of the McMurdo Volcanic Group.

2.2. Study area

Our study is located in part of northern Victoria Land between the Bowers Mountains and the Lanterman Range (Ob Bay and Mt. Soza quadrangles), inside the Bowers terrane (Fig. 2). Previous work here has mainly focussed on the Lanterman Fault zone, a site of recurrent deformation and complex structural evolution. The following large-scale deformation events have been described in the literature:

- The main phase of ductile suturing between the Wilson and Bowers terranes occurred at amphibolite/greenschist facies conditions (Capponi et al., 1999) during the Ross Orogeny (Di Vincenzo et al., 1997; Goodge, 2007);
- This early suturing is postdated by a phase of sinistral strike-slip shearing in the Lanterman Range dated at 480–460 Ma (Crispini et al., 2007b). It, therefore, represents a late- to post-Ross Orogeny deformation event.
- Cenozoic tectonics: a NW–SE to NNW–SSE trending dextral strike–slip to oblique slip regime is thought by many authors (e.g., Salvini et al., 1997; Rossetti et al., 2003) to be responsible for the formation of the Rennick Graben which lies immediately to the west of the study area. A major bend of the main fault zone from NNW–SSE to NW–SE/E–W in the Lanterman Range area was thought to have caused a change from transtension- to transpression-dominated dextral shearing, with associated positive flower structures. Maximum principal stresses (σ_1) are thought to trend N–S to NNW–SSE (Rossetti et al., 2002).

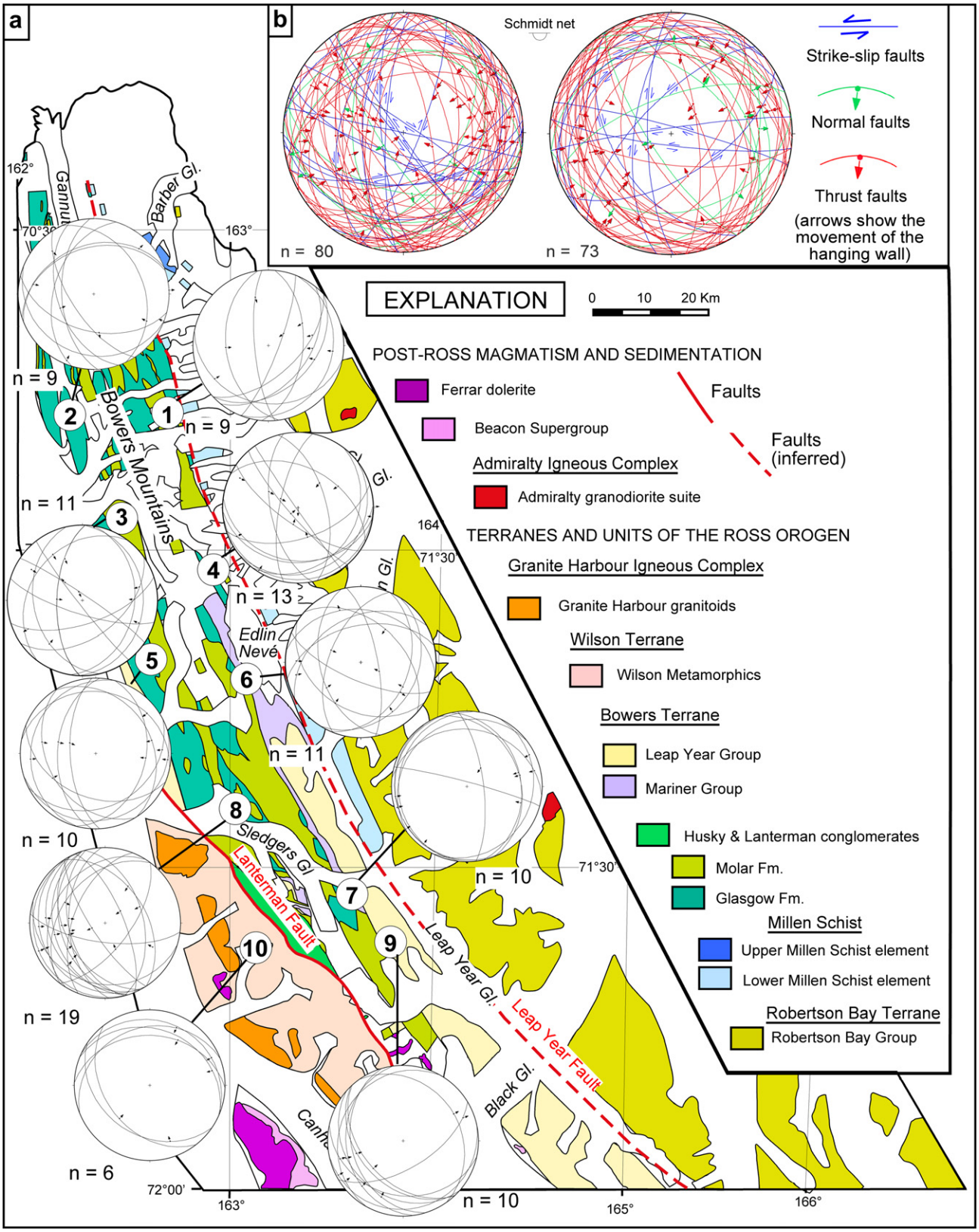

Fig. 2. (a) Geologic map of the study area and location of the structural stations for fault–slip analysis with stereoplot showing fault data selected by the software as pertaining to the local dominant fault system; (b) stereoplot showing all collected fault data for the northern and southern studied sector. All stereoplots are equal-area projections, lower hemisphere.

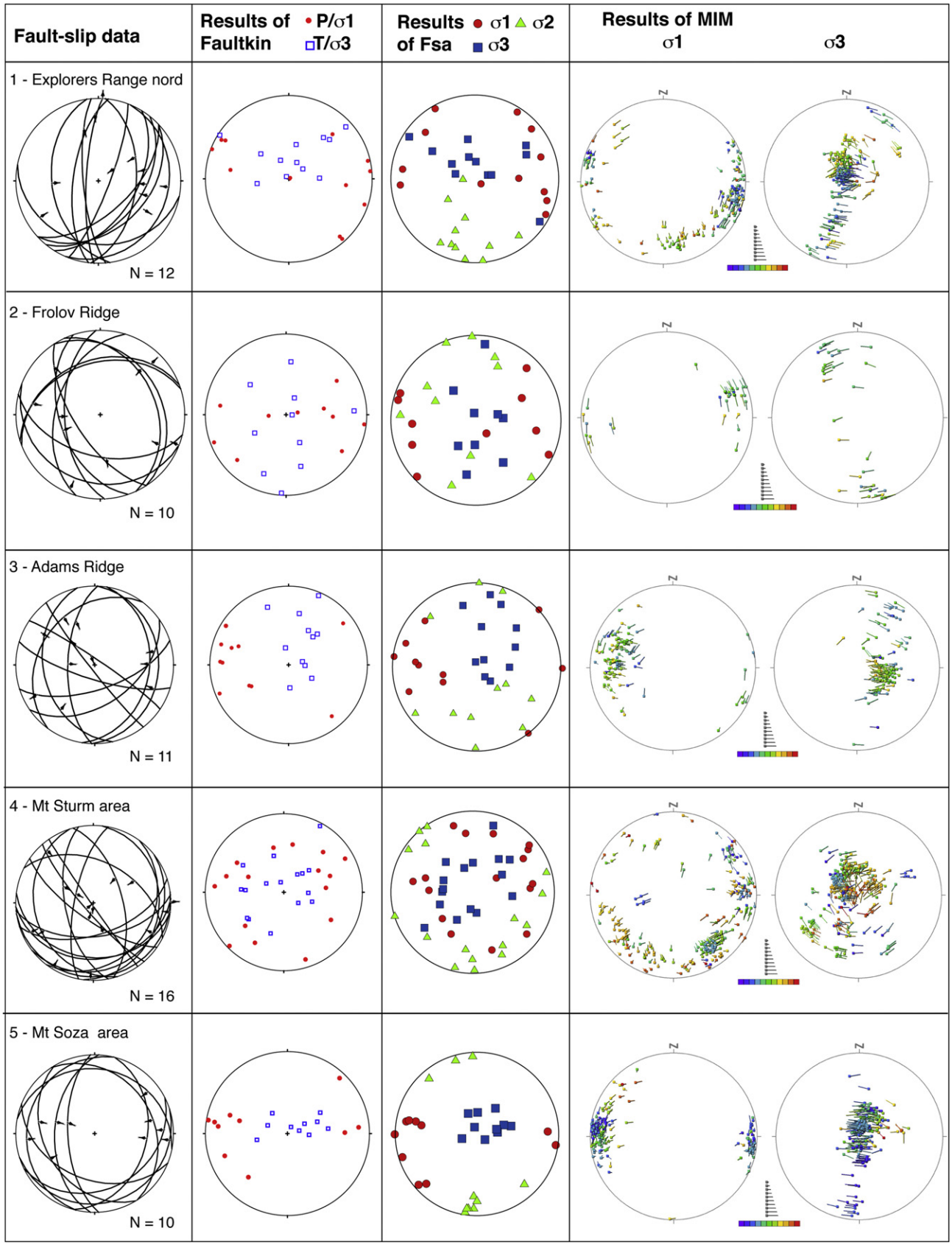

Fig. 3. Compilation of measured data and results of Faultkin, FSA and MIM, all methods applied to the entire fault population of a single location. All stereoplots are equal-area projections, lower hemisphere.

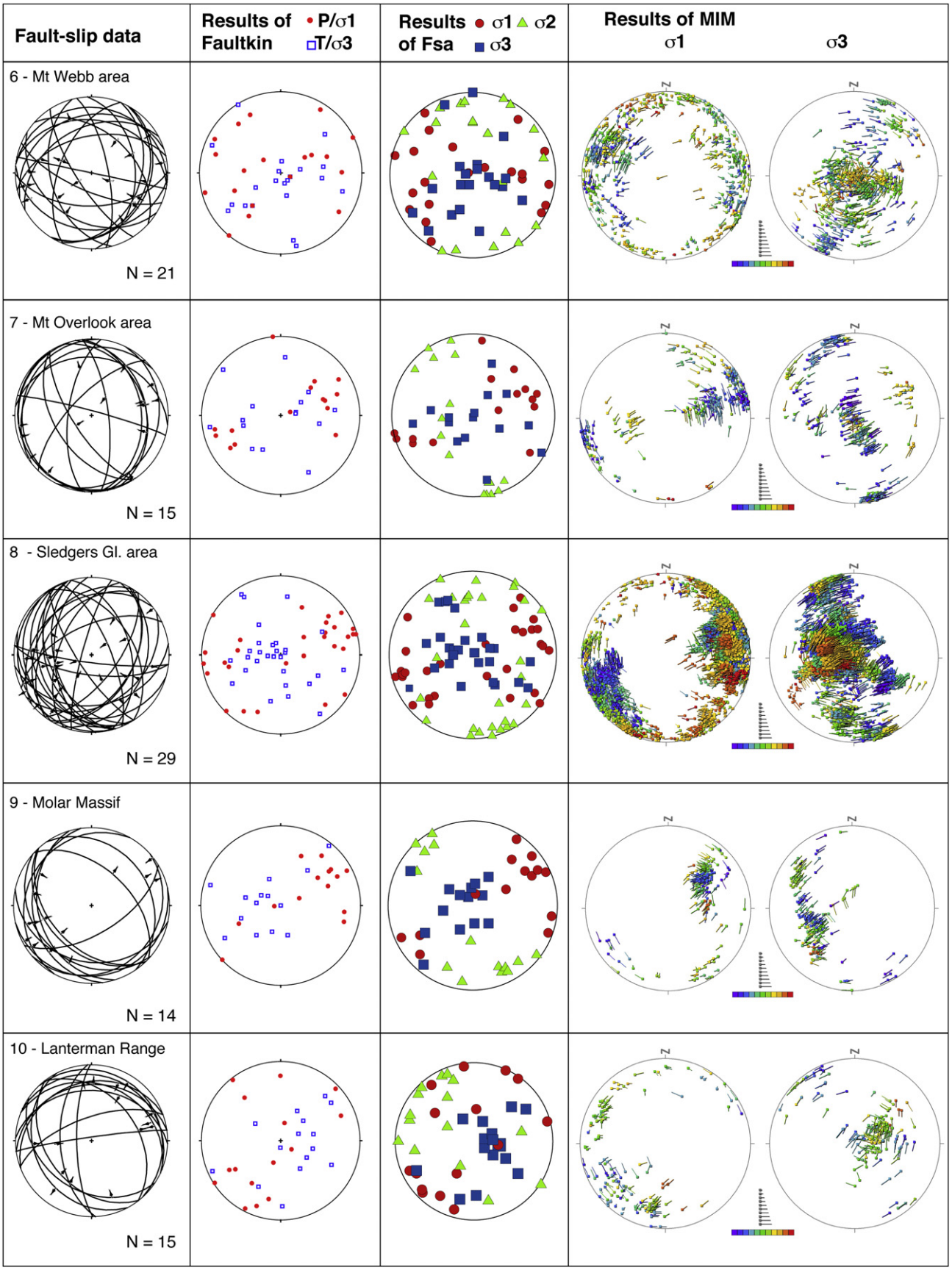

Fig. 3. (*continued*).

Less detailed work exists for the Leap Year Fault. Salvini et al. (1997) and subsequent work by the same research group interpret it as another right-lateral strike–slip fault linked to Cenozoic tectonics. By contrast, Crispini et al. (2007a) suggest a left-lateral oblique–slip motion of post-Ross orogenic age; multiple reactivations are possible.

Importantly, there is also evidence of tectonic activity between the end of the Ross Orogeny and intrusion of the Devonian–Carboniferous Admiralty plutons: this includes post-Ross (less than 375 Ma) K–Ar whole-rock ages from slates and schists close to the two main faults reported by Adams (2006), greenschist–facies deformation at about 360 Ma close to the Bowers/Robertson Bay terrane boundary (Capponi et al., 2002) and shear zone deformation in the inboard Wilson Terrane at about 440 Ma (Di Vincenzo et al., 2007). In spite of such evidence, the overall tectonic scenario for the time period between the Ross Orogeny and the Admiralty pluton emplacement remains unclear.

3. Field data

We investigated the mesoscale fault pattern in the area of the Bowers Mountains between the Lanterman Fault and Leap Year Fault (Figs. 1 and 2). We collected fault–slip data from 153 striated fault planes at 10 localities (Fig. 3), scattered between 70°45′–71°45′ Lat. S and 162°00′–163°45′ Long. E (Fig. 2).

In the study area the sparse number of outcrops of Devonian–Triassic sediments (Beacon Supergroup) and/or Jurassic rocks (Ferrar Dolerite and Kirkpatrick Basalt) make finding age constrains for the brittle structures difficult. In order to constrain the possible age interval of fault activity to Early Paleozoic, we selected fault sets that are postdated by intrusion of the Admiralty plutons or Gallipoli volcanics located close to the study area and excluded all the younger fault sets that affect them. We observed that some of the faults sutured by the Admiralty intrusives develop diagnostic damage zones and associated mineralization suites, i.e., diffuse quartz–carbonate veining (locally epidote-rich) and hydrothermal alteration. We then used this criterion to date other structures on the assumption that all faults exhibiting such mineralization features belong to the same pre-Admiralty set. In addition, the overprinting relationships indicate that these faults systematically belong to the oldest set where different fault systems are present in specific outcrops. The characteristics of such faults do not match those of the much later Cenozoic structures described by several authors (e.g., Salvini et al., 1997; Rossetti et al., 2003).

All faults clearly postdate the ductile structures (foliation and folds) linked to the Cambro-Ordovician deformation during the Ross Orogeny (Wodzicki and Robert, 1986; Jordan et al., 1984). The foliation is a pervasive composite fabric parallel to the axial planes of regional F_1 folds (Wodzicki and Robert, 1986) with curved hinge lines, plunging both to the NW and to the SE, controlling the location and geometry of the mapped lithological contacts. The regional foliation strikes N–S in the northern part of the study area and NW–SE in the southern part (Sledgers Glacier area) (Fig. 4). This change is linked to a superposed deformation characterized by open fan-shaped F_2 folds and sinistral shear accommodated by the development of NNW–SSE regional shear zones. (Capponi et al., 1999).

The studied brittle structures form a complex pattern of shallowly-dipping reverse faults with different orientations (Figs. 2 and 3), that are closely associated with NNW–SSE striking, steeply-dipping strike-slip faults, that are dominantly sinistral. Frequent oblique–slip faults with a reverse component have been documented, together with subvertical reverse faults and locally developed positive flower structures (Fig. 5a–c).

The main fault system changes strike and tectonic transport direction moving from the northern to the southern sector of the study area. In the north, strike-slip faults have N–S trends and thrust

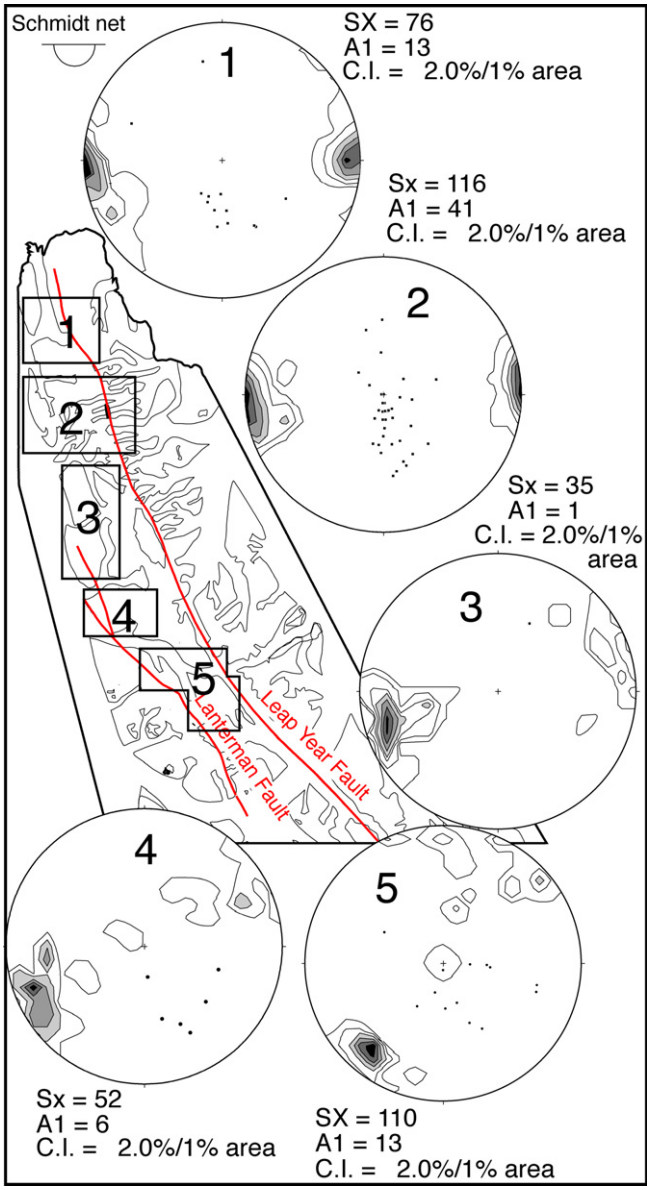

Fig. 4. Tectonic sketch showing density plots for Sx (regional fabric) and A_1 (axis of F_1) in the study area (from original and literature data).

faults show top-to-E and top-to-W shear senses. To the south, steeply-dipping sinistral strike-slip faults tend to strike NW–SE and conjugate low-angle reverse faults have top-to-NE and top-to-SW sense of shear. This fault system is locally overprinted (especially in the Lanterman Fault area, Capponi et al., 1999) by subvertical N–S to NNW–SSE strike-slip faults with right-lateral senses of shear.

One of the characteristic features of the investigated fault system is the development of damage zones containing mineral vein networks, hydrothermally altered epidote–chlorite rocks and wallrock alteration zones (Figs. 5d and 6). In places, the occurrence of hydraulic breccia and jigsaw puzzle textured veins or breccia veins in the fault zones testifies to tectonic events accompanied by hydrofracturing (e.g., Woodcock and Mort, 2008). Repeated fluctuations in fluid pressure are inferred from the widespread occurrence of laminated crack–seal veins (Ramsay, 1980; Sibson et al., 1988).

Two main vein compositions occur: (i) epidote-rich, quartz–carbonate veins, with minor prehnite and/or pumpellyite; and (ii) quartz–carbonate veins with sulphides, accompanied by diffuse

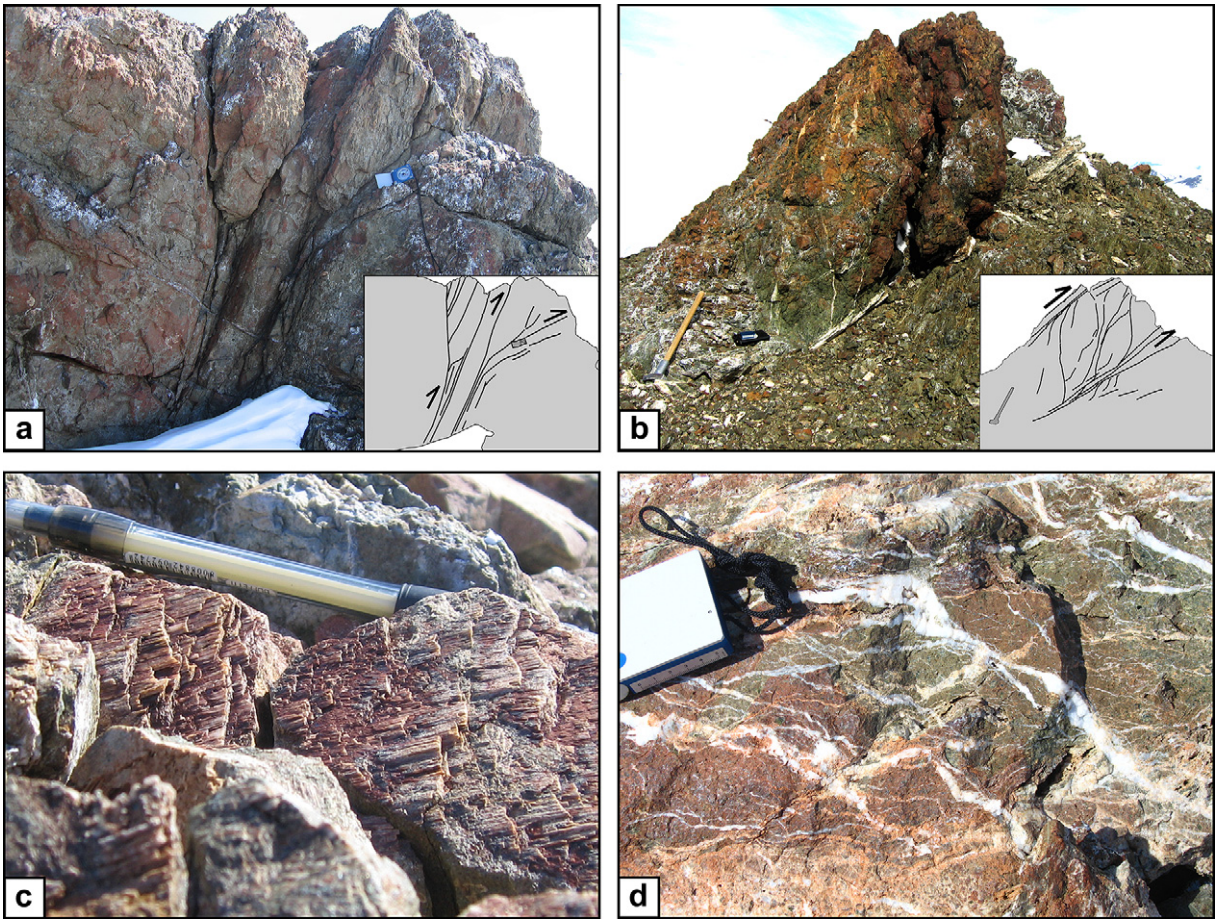

Fig. 5. Field examples of studied brittle structures: (a) outcrop scale positive flower structure in Glasgow metavolcanics (view towards the north; Bowers Mountains north of Mt. Overlook); (b) thrust fault zone with minor imbricate structures (Glasgow metavolcanics, south of the Sledger Glacier); (c) slickenfibres composed of quartz, chlorite and epidote (Glasgow metavolcanics, North of the Sledger Glacier); and (d) damage zone in partially recrystallized metabasalt with intense quartz veining (Glasgow metavolcanics, North of the Sledger Glacier).

wallrock alteration. In one location gold mineralization occurs (Crispini et al., 2007c; Crispini et al., in press).

Overall, the development of mineral vein networks and wallrock alteration zones is consistent with substantial amounts of syn- to post-tectonic fluid circulation and rock–fluid interaction, with temperature estimates from chlorite thermometry suggesting ranges from 270 to 320 °C (Crispini et al., 2007c).

4. Methods

4.1. Inversion of fault–slip data

Most fault–slip inversion techniques use one or two fundamental assumptions:

- They impose a geometrical constraint requiring that slip on the fault plane takes place parallel to the direction of maximum resolved shear stress (Wallace, 1951; Bott, 1959, so-called "Wallace–Bott hypothesis"),
- Alternatively or additionally, they include a frictional constraint that the fault plane must form with an orientation that fulfils the Mohr–Coulomb yield criterion, e.g., the shear-to-normal stress ratio equals $\tan\varphi$ where phi is the angle of internal friction (Coulomb, 1776).

Using these constraints, different methods have been proposed to solve the inversion problem, that is, to derive the reduced stress tensor from measured fault–slip data. Some techniques use the geometrical criterion whilst others rely on the frictional criterion; some combine both approaches (Célérier, 1988; Angelier, 1990; Zalohar and Vrabec, 2007). The latter group of methods are particularly valuable since those based solely on the geometrical constraint allow mechanically unacceptable solutions, such as fault plane orientations with a very small shear stress combined with a very large normal stress (Célérier, 1988). Comprehensive reviews of the different techniques are given in Angelier (1994), Ramsay and Lisle (2000) and Liesa and Lisle (2004).

To obtain solutions that are as realistic as possible, we combined different approaches using different software packages.

4.1.1. Faultkin

The software Faultkin 4.3.5 (Allmendinger et al., 1994) uses the '*P* and/or *T* Dihedra Grid' graphical/analytical method proposed by Angelier and Mechler (1977) and Angelier (1979, 1984). This method is founded on the Wallace–Bott hypothesis and calculates *P*, *B* and *T* axes as defined in seismology (Scheidegger, 1964). The *P* and *T* axes are constructed by bisecting the orthogonal nodal planes of a fault plane solution, and thus lie at 45° to those planes (Marrett and Allmendinger, 1990). They are kinematic axes and correspond to the principal directions of incremental strain (see Marrett and Allmendinger, 1990). We refer to them below simply as the maximum shortening axis (*P*), the maximum stretching axis (*T*) and the intermediate axis (*B*). In many cases, they represent reasonable approximations of the principal stress axes; for a detailed discussion of this topic see Célérier (1988).

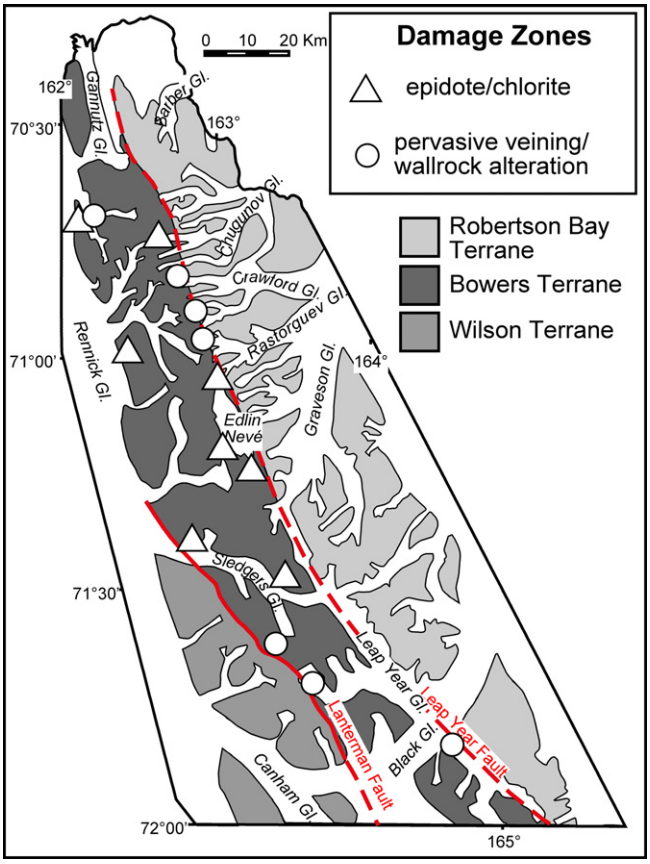

Fig. 6. Sketch map of the study area with the location of the damage zones where the observed hydrothermal alteration and veining is more intense.

4.1.2. MIM (Multiple Inverse Method)

MIM is a modification of the classic inverse technique of Angelier (1984), and thus is based on the geometrical criterion (Yamaji, 2000). This method has been created specifically to derive stresses from heterogeneous fault–slip data, and, therefore, follows a step-by-step procedure: first, it creates groups of k elements from the whole data set (Yamaji et al., 2005a). If $k = 4$, it generates each possible set of 4 faults so that each fault is related to any possible combination of three other faults. Then it applies Angelier's (1984) inverse technique to all of these artificial k-fault subsets. Finally, all calculated reduced stress tensors, i.e., one for each 4-fault-subset in our example, are plotted in lower-hemisphere plots, one for σ_1 axes and the other for σ_3 axes (Yamaji and Sato, 2005). Symbols of different colours refer to different values of the ratio $\Phi = (\sigma_2 - \sigma_3)/(\sigma_1 - \sigma_3)$.

With this procedure, we are theoretically able to appreciate all significant stress states inherent in a heterogeneous data set, as they are indicated by clusters of symbols that agree in terms of σ_1- and σ_3-directions as well as colours (see, for instance, Fig. 3).

To filter the solutions, the enhance factor e (with $0 \leq e \leq 99$) defines a threshold value which is required for a particular stress state to appear in the MIM stereograms (Yamaji et al., 2005b).

If you select $e = 0$, all solutions for a data set are plotted. Larger values of e, on the other hand, correspond to a reduced number of plotted solutions and are chosen to enhance the most relevant clusters.

4.1.3. FSA

The FSA software (Célérier, 1999 and subsequent modifications) is based on a combination of both the geometrical and frictional constraints.

It first calculates a large number of reduced stress tensors by means of a random grid search. The reduced stress tensor is used to predict the slip for each fault, which is then compared to the real slip on each fault plane. The difference between these two values, indicated as the 'misfit angle', represents a measure of quality of the tensor solution with respect to how well it fits the actual fault–slip data. The best tensors are, therefore, those that minimize the deviation between the shear stress and the measured slip on fault surfaces.

Secondly, it investigates which of these tensors also satisfy the frictional constraint. FSA permits a direct inspection of the reduced Mohr circle resulting from the different calculated stress tensors, allowing the user to choose the one with the largest number of faults showing high shear stress to normal stress ratio. These faults tend to be tangent to the external (σ_1–σ_3) circle and are probably neoformed in the investigated stress field.

4.2. Procedure of analysis

We carried out a preliminary inspection of the fault–slip data by applying Faultkin, FSA and MIM routines to the whole data set of single outcrops. Results show a moderate degree of heterogeneity of the database (Fig. 3) as indicated by dispersion of both calculated σ_1 and σ_3 axes (for FSA and MIM) and kinematic axes (for Faultkin).

To unravel these data sets, we adopted a stepwise procedure, as suggested by Sippel et al. (2009); in particular:

(1) We first applied the '*P* and/or *T* Dihedra Grid' method to the whole data set for a single outcrop using Faultkin and then performed a visual inspection to eliminate fault data that don't fit;
(2) We then apply the FSA routine to the same data set and select the stress tensor that satisfies the largest number of faults using a threshold value of the misfit angle of 40° as a first approximation (we refer to this restricted database as the "first subset db");
(3) We then sequentially apply Faultkin and FSA to the first subset db; in this second run, misfit angles are usually less than 20°, with few fault data between 20° and 30°. A good quality result is also indicated by the shape of the angular deviation histogram: the best solutions usually show the maximum of the histogram corresponding to the smallest differences in angle. Moreover, the calculated stress tensor is also evaluated through the inspection of the Mohr circle: stress tensors that are characterized by higher shear stress/normal stress ratio (and, therefore, with faults plotting near to the outer circle) are preferred; these stress tensors are reported in Table 1.
(5) We apply MIM to the whole data set for a single outcrop, using $e = 5$, to compare results of the different routines;
(6) We then perform a second run of MIM on the first subset db using $e = 50$ using the stress tensor identified by Faultkin, and
(7) we finally apply MIM to the first subset db using $e = 50$ using the stress tensor identified by FSA.

We group the faults excluded from the first subset db in a "second subset db" and we repeat the procedure from 1 to 7. There are usually faults that cannot be assigned to any tensor; they may represent stress states related to few measured faults; if less than 4 fault–slip data are present, the procedure of inversion cannot theoretically constrain any stress tensor (e.g., Célérier, 1988 and cited references), and, as a consequence, we evaluate them at the end of the routine.

At the end of the analysis, we compare results of the different software packages against each other and with the field observations. In particular, we try to establish the relative chronology of the

Table 1
Results of separation and inversion of fault–slip data for each location. All stereoplots are equal-area projections, lower hemisphere. ($r_0 = (\sigma_1 - \sigma_2)/(\sigma_1 - \sigma_3)$; $F = (\sigma_2 - \sigma_3)/(\sigma_1 - \sigma_3)$).

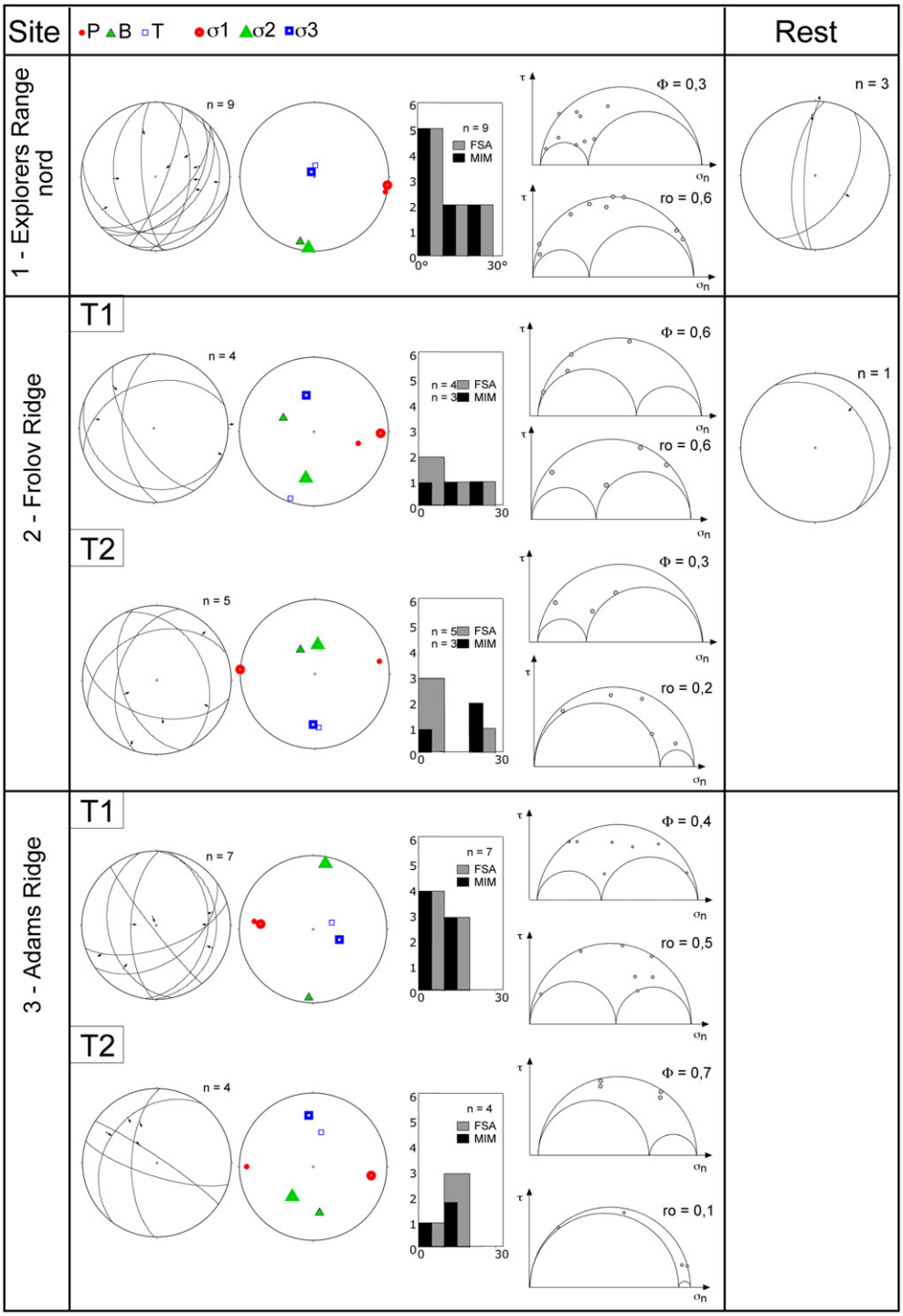

(*continued on next page*)

calculated stress tensors using locations where overprinting relationships have been observed in the field.

By way of an example, consider structural station 6, which comprises 21 fault–slip data. When Faultkin is applied to the whole data set, it reveals quite a big scatter (Fig. 7a). Visual inspection suggests that we could exclude 8 data, but this procedure is highly subjective and involves a high degree of error. Therefore, we performed the first run with FSA software and exclude 14 faults that have a misfit angle higher than 40° (Fig. 7b). The seven remaining data represent the "first subset db" for structural station 6. On this reduced data set we perform a second run with FSA: now the misfit angles do not exceed 20° and the calculated stress tensor is

Table 1 (*continued*)

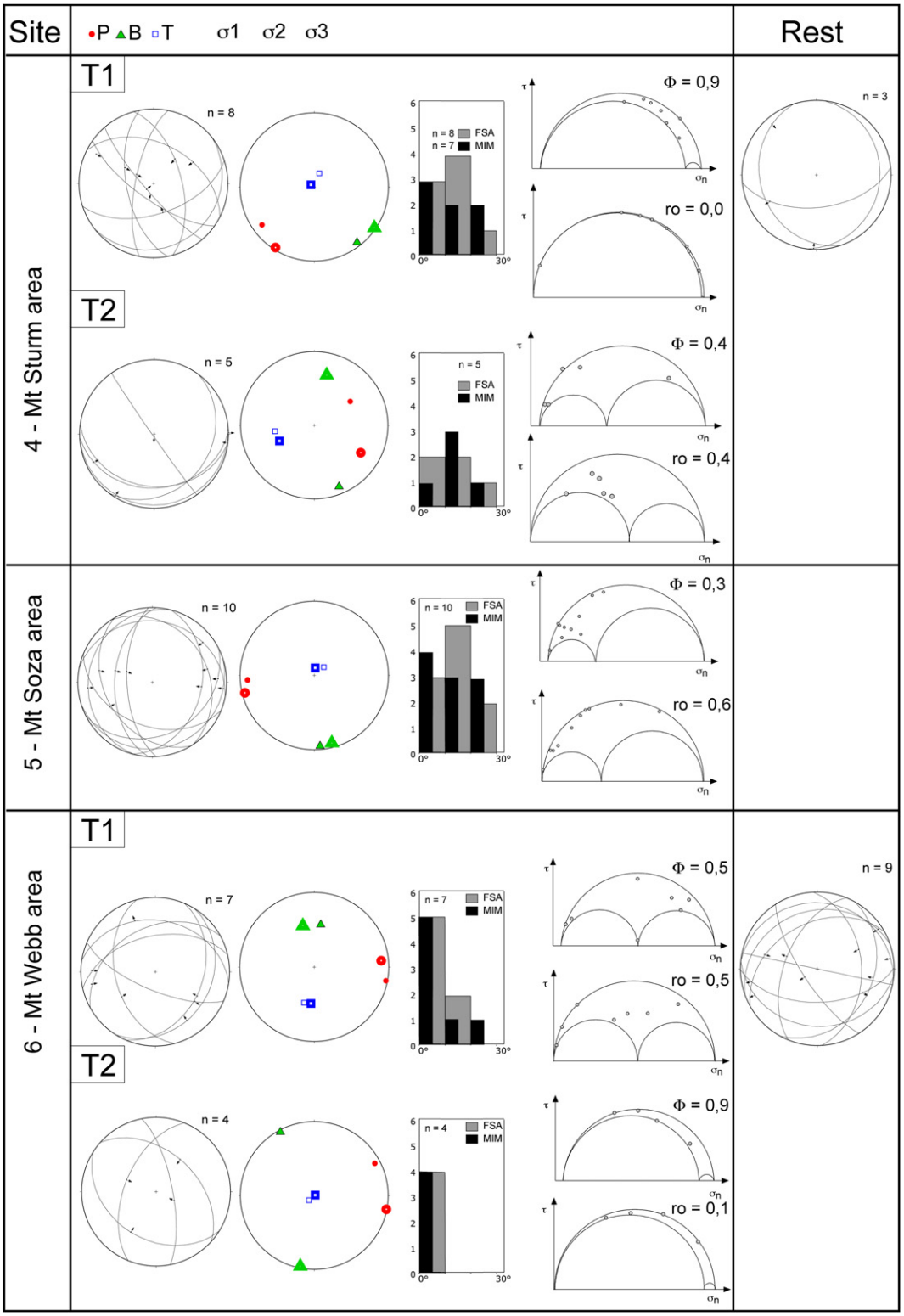

compressive/transcurrent with an E–W trending σ_1 (Fig. 7c). For this stress tensor, FSA calculates an aspect ratio $r_0 = 0.48166$, with $r_0 = (\sigma_1 - \sigma_2)/(\sigma_1 - \sigma_3)$. The Faultkin result agrees with FSA and shows an E–W trending P axis and an aspect ratio of the strain ellipsoid R of 0.38778, where $R = (E_2 - E_3)/(E_1 - E_3)$.

When MIM software is used to analyse the whole data set, it once again produces a high degree of scatter (see Fig. 3), and the result does not enable the identification of a stress tensor with reasonable confidence. However, when applied to the first subset db, we obtain results whose orientations are consistent with those

Table 1 (*continued*)

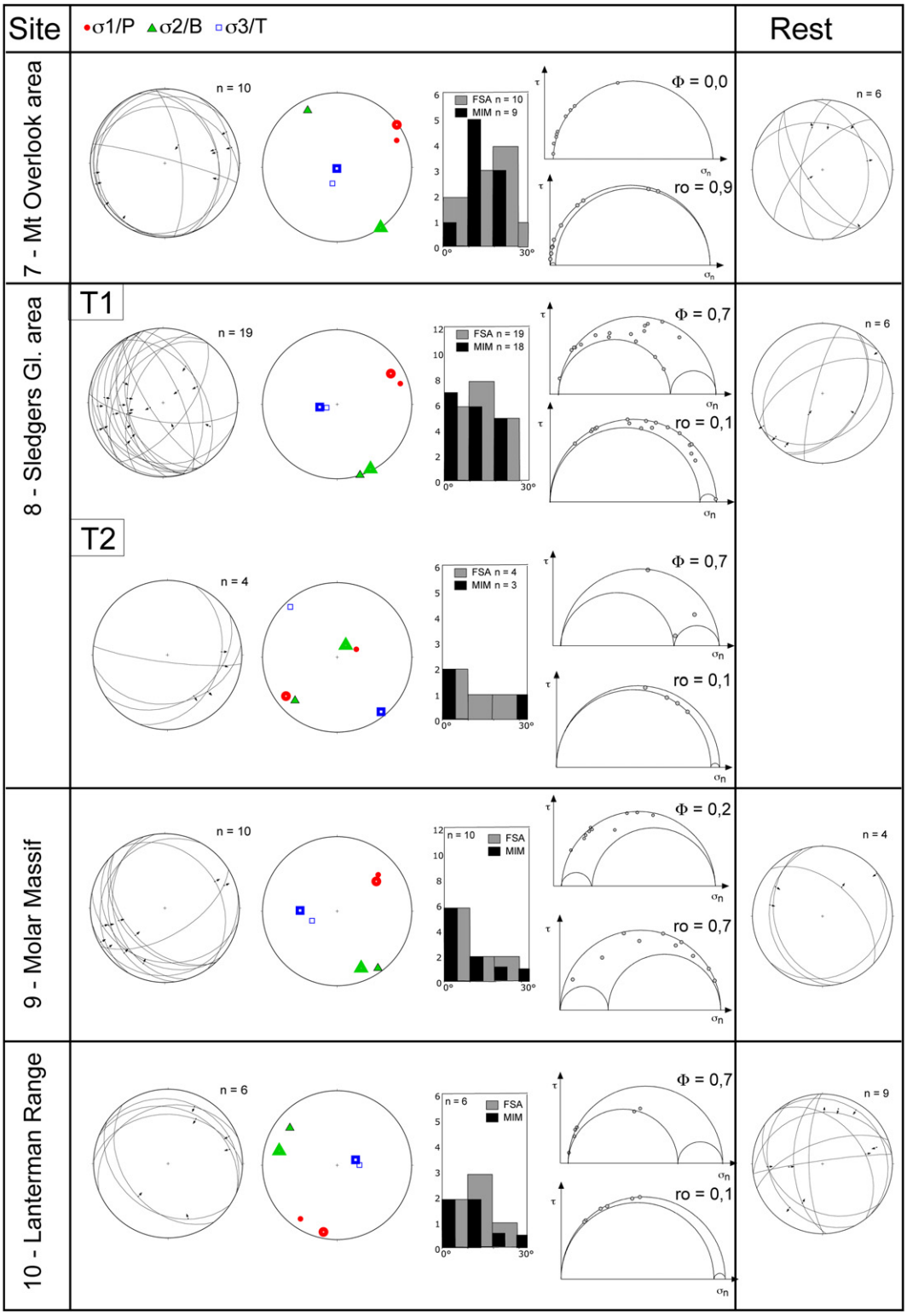

obtained using the other software packages (Fig. 7d). The different colours of the tadpoles in Fig. 6d refer to different values of Φ, so we still have to choose the Φ factor ($\Phi = (\sigma_2 - \sigma_3)/(\sigma_1 - \sigma_3)$) for the MIM stress tensor. To do this we superimpose the P–T axes and the stress axes derived from the Faultkin and FSA calculations, respectively, on the tensors calculated by MIM (Fig. 7d), as suggested by Sippel et al. (2009). In this case $\Phi = 0.5$ (light green) for the FSA tensor and 0.6 if we use the P–T axes calculated by Faultkin. We then check

the chosen tensors with the database of fault–slip data. The misfit angles calculated by MIM using the stress axes calculated with FSA are low (lower than 20°, apart from one value of 24.9°), as shown in Fig. 7e. In this structural station, and in general, better agreement exists between MIM and FSA results than between MIM results and *P*–*T* axes calculated by Faultkin.

Following the same procedure with the remaining faults, we identified a second subset db comprising 4 data. This subset fits a stress tensor that is almost purely compressive, again with E–W trending σ_1. There are now 10 faults that don't fit any of the calculated stress tensors.

The shear-to-normal-stress ratios used to draw the reduced Mohr diagram for the best-fitting stress tensor are directly calculated by FSA, whereas for MIM tensors, we used the software FLUMO (Sperner et al., 1993).

5. Results

Most of the fault populations are heterogeneous, as illustrated by the different orientations of strain axes calculated by Faultkin and of stress axes calculated from FSA and MIM (Fig. 3). Where possible, we have separated different subsets (whose significance is discussed below), whilst in other cases, if the data set was too small, just one stress tensor was calculated, or the faults don't fit, they have been grouped in the "Rest" column of Table 1. For each stress tensor we show the misfit angles (fluctuation histograms) of both FSA and MIM solutions and the corresponding reduced Mohr diagrams. Since the procedure of inversion of fault–slip data only allows us to calculate the directions of the principal stress axes and the ratios of the principal stress differences ($r_0 = (\sigma_1 - \sigma_2)/(\sigma_1 - \sigma_3)$ or $\Phi = (\sigma_2 - \sigma_3)/(\sigma_1 - \sigma_3)$), the shape of the Mohr diagram is known, but the absolute size and position remain unknown.

5.1. Results of fault–slip analysis for each structural station

Results of fault-slip analysis are shown in Table 1.

1) Structural station 1
Nine faults define a compressive stress tensor with an E–W trending σ_1. The FSA and MIM results show a good agreement, both in terms of the orientation of the principal stress axes and the stress tensor aspect ratio. However, the reduced Mohr diagram for the FSA tensor is better defined.

2) Structural station 2
Two different tensors are calculated, each based on a few data. Both show an E–W trending σ_1. In detail, one tensor is characterized by inverted positions between σ_2 and σ_3 in Faultkin and FSA results. Both tensors show a certain degree of obliquity. One in particular has σ_2 plunging between 56 and 58 degrees. The stress tensor orientation remains essentially constant, but the principal stress magnitudes vary due to the maximum and intermediate stresses swapping positions. These two tensors could represent different superposed events, but the persistency of similar σ_1 orientation may be better explained with a stress field with compressive and strike–slip components.

3) Structural station 3
An E–W trending, dominantly compressive tensor is calculated. A second, more oblique tensor, with similar σ_1 is defined by 4 faults. One of these faults may be the reactivation (double slickenline) of an older fault, thereby giving a sequence to the tensors. The second tensor is characterized by higher Φ (and consistently lower r_0) values. The persistency of similar σ_1 orientations points to local reactivation in the framework of the same stress field.

4) Structural station 4
A compressive stress field with a NE–SW trending maximum compressive stress is calculated on the basis of either 8 (FSA) or 7 (MIM) faults. Unlike station 3, the purely compressive tensor here shows a very high Φ (and low r_0) value. The other 5 data define a second oblique stress tensor: in this case *P*–*B*–*T* axes and FSA-calculated σ_1 and σ_2 are 53° apart.

5) Structural station 5
All data in this station fit a compressive tensor with an E–W trending σ_1.

6) Structural station 6
An oblique/compressive stress tensor with an E–W trending σ_1 is calculated by all software methods; four other data fit a second genuinely compressive stress tensor with an E–W trending, subhorizontal σ_1. Like structural station 4, the genuinely compressive tensor shows a very high Φ (and low r_0) value. Again the similarity of σ_1 orientation points to local rotations of the stress tensor in the framework of the same stress field.
Normal sense reactivations of older reverse/oblique–slip faults is observed in the field: these normal faults don't fit any of the calculated tensors.

7) Structural station 7
A compressive stress tensor with a NE–SW trending σ_1 is calculated.

8) Structural station 8
A compressive stress tensor with a NE–SW trending σ_1 is calculated. A second stress tensor is recognized, that is dominantly strike–slip according to FSA and dominantly normal according to *P*–*B*–*T* axes. The two results have σ_1/*P* axis and σ_2/*B* axis reciprocally inverted and are based on few data. However, a fault belonging to this system cross-cuts one of the reverse faults of the first tensor and, therefore, a local time sequence can be established.

9) Structural station 9
A dominantly compressive, slightly oblique stress tensor is calculated, with a NE–SW trending σ_1.

10) Structural station 10
A compressive stress tensor with a NNE–SSW trending σ_1 is calculated.

5.2. Shapes of the strain ellipsoids

Since *P*, *T* and *B* axes calculated by Faultkin are related to the principal incremental strain axes, we can measure the shape of the strain ellipsoid using the ratio:

$$R = (E_2 - E_3)/(E_1 - E_3)$$

where E_1, E_2 and E_3 are the eigenvalues of the Bingham moment tensor (Table 2).

Values of 1.00, 0.50 and 0.00 for *R* indicate ideal flattening, plane–strain and constrictional ellipsoids, respectively. In a more general way, we can suggest (see for instance Diraison et al., 2000) that values between 0.35 and 0.65 indicate a plane–strain type (stations 1, 2 T2, 4 T2, 5, 6 T1, 8 T1, 9, 10), whilst values between 1.00 and 0.65 indicate a strain ellipsoid of flattening type (stations 2 T1, 3 T1, 7) and values between 0.00 and 0.35, a constrictional type (stations 3 T2, 4 T1, 6 T2).

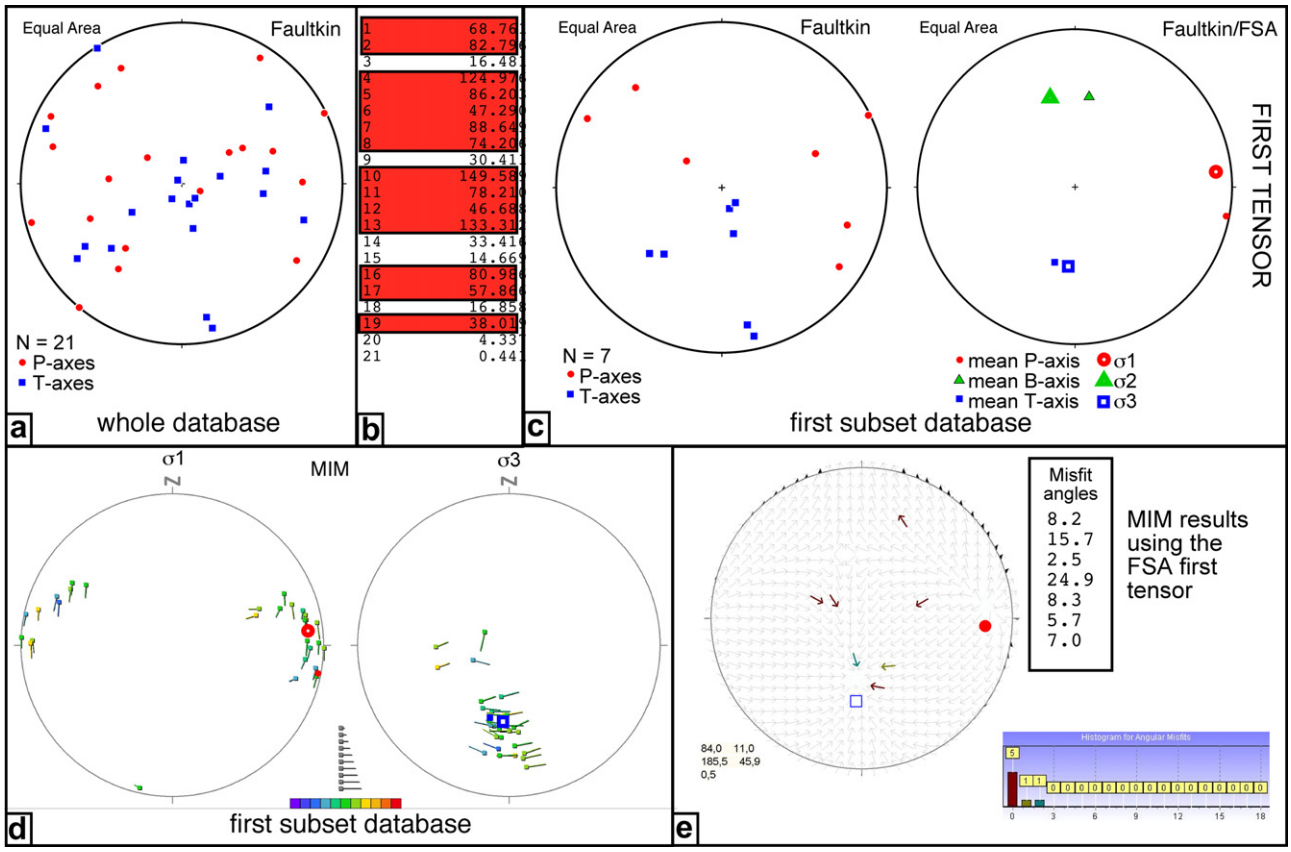

Fig. 7. Example of the stepwise procedure of fault–slip analysis for structural station 6 (see text for explanation).

6. Discussion

6.1. Paleostress inversion method

A good agreement exists between stress calculations and field data. All the reactivated faults identified in the field were either assigned to two different stress tensors or were assigned to one stress tensor and to the "rest" group by the software. In contrast, when single fault planes with a curved geometry have been identified (4 cases), the software was able to fit them into the same stress tensor in just one case. As a consequence, caution needs to be taken performing analysis of fault–slip data in areas of transpressive or transtensive tectonics, where faults commonly changing dips from deeper to shallower levels.

Table 2
Eigenvalues for *P*, *T* and *B* axes (E_3, E_1 and E_2, respectively) and calculated ratio $R = (E_2 - E_3)/(E_1 - E_3)$.

	*E*1	*E*2	*E*3	*R*	Type
Stop1 1T	0.35	−0.01054	−0.341	0.47823444	Plane strain
Stop2 1T	0.15	0.06376	−0.214	0.76307692	Flattening
Stop2 2T	0.31	−0.04102	−0.269	0.39374784	Plane strain
Stop3 1T	0.32	0.07228	−0.4	0.65594444	Flattening
Stop3 2T	0.38	−0.11	−0.269	0.2449923	Constrictional
Stop4 1T	0.35	−0.107	−0.25	0.23833333	Constrictional
Stop4 2T	0.43	0.03532	−0.436	0.54424942	Plane strain
Stop5 1T	0.35	−0.04936	−0.309	0.3939909	Plane strain
Stop6 1T	0.3	−0.04162	−0.258	0.38777778	Plane strain
Stop6 2T	0.44	−0.139	−0.309	0.22696929	Constrictional
Stop7 1T	0.2	0.05357	−0.254	0.67746696	Flattening
Stop8 1T	0.34	−0.01961	−0.327	0.46085457	Plane strain
Stop9 1T	0.33	0.04875	−0.38	0.60387324	Plane strain
Stop10 1T	0.42	−0.06163	−0.364	0.38567602	Plane strain

By comparing the Mohr diagrams produced through the FSA and MIM software packages (Table 1) we notice that stress fields calculated by FSA usually give rise to a higher shear/normal stress ratio, that is a higher slip tendency, for a larger number of faults compared to the MIM results. This probably means that the routine followed by the MIM software does not always yield the most realistic stress states for a given fault population.

A good agreement between FSA and MIM results exists for the great majority of Φ/r_0 ratios of the different stress tensors.

Faultkin is not able to separate different strain tensors in a heterogeneous data set, but a first-order similarity exists between kinematic axes calculated by Faultkin and FSA stress axes. This seems to confirm its validity for a rapid inspection of fault–slip data.

MIM often generates large and diffuse clusters for the different subsets and, therefore, the identification of the relevant stress states is not always straightforward.

6.2. Stress regimes

In many of the investigated locations, different methods of fault–slip analysis identify just one stress tensor. When the paleostress calculations resulted into two stress tensors, the orientation of σ_1 usually remains stable (structural stations 2, 3, 4, 6), whereas σ_2 and σ_3 may vary in the plane perpendicular to σ_1, ranging from almost pure compressive stress regimes to variable degrees of wrench component. In these cases we attributed both the stress tensors to the same stress regime.

The dominant stress regime of the studied area is characterized by an E–W to NE–SW trending subhorizontal σ_1. A progressive rotation from E–W to NE–SW directions occurs from north to

south (Fig. 8), in accordance with the changing orientation of the pre-existing ductile regional fabric. The presence of an inherited structural anisotropy in the study area implies that the lithosphere likely behaved anisotropically to subsequent brittle deformations; i.e., planes of weakness were not randomly distributed. This potentially disturbs paleostress determinations. However, calculated stress tensors (especially those from FSA, see Table 1) appear to induce relatively high shear-to-normal-stress ratios on the respective faults (these plot near the outer envelope of the associated Mohr circles). This indicates that many faults contain the σ_2-axis in their plane, something that may imply a neoformed character. This is also favoured by the fact that we have not analyzed the main bounding faults (Lanterman and Leap Year faults), but minor structures in between.

Only in the Sledgers Glacier area (structural station 8) does a likely younger tensor occurs, that can be linked either to a strike-slip or to a normal regime, with a NE–SW trending σ_1. In the framework of a sinistral E–W trending strike–slip system normal faults can develop as an en echelon array of *T*-fractures (Tchalenko and Ambraseys, 1970). We, therefore, favour the strike–slip tensor over the normal tensor. Since the σ_1 direction remains constant with the compressive tensor, and the tensor is calculated from only four data, its geological significance remains unclear. However, field evidence of cross-cutting relationships between the two fault sets belonging to the different tensors may indicate a local rotation of the stress field in the area north of the Lanterman Range.

6.3. Significance of compressive oblique stress field

The remarkable consistency in the orientations of the calculated stress tensors in different locations points to the development of a regionally significant obliquely compressive deformation regime, i.e., transpression.

The main fault zones are NNW–SSE to NW–SE striking and the relationships between the attitude of σ_1 and the main fault zones (Fig. 8) define a transpression zone with sinistral kinematics. Transpression is also suggested by frequent presence in the field of curved fault surfaces with positive flower geometries (Fig. 4a). The swapping of stress (or strain) tensor orientations as seen for instance in structural station 2, is again a feature commonly observed in transpressional geometries (e.g., Audemard et al., 2005).

Transpression (Harland, 1971; Sanderson and Marchini, 1984; Fossen and Tikoff, 1993; Robin and Cruden, 1994; Dewey et al., 1998; Holdsworth and Pinheiro, 2000; Holdsworth et al., 2002; Tavarnelli et al., 2004) often develops in response to oblique convergence across pre-existing regional-scale discontinuities. A partitioning between dip–slip reverse and strike–slip faulting is common (e.g., Fossen and Tikoff, 1993) and allows the accommodation of both the lateral displacement due to the convergence obliquity and the shortening relative to the perpendicular plate convergence. This would also explain the compatibility that exists in our case study between reverse and strike–slip faults. A combination of distributed thrusting and wrenching is also confirmed by the shapes of the strain ellipsoids (dominantly flattening to plane strain types; Merle and Gapais, 1997).

Stress inversion techniques in transpressional deformation zones need to be applied with a high degree of caution, because of high frequency of “non-Andersonian” faults. However, many examples exist where the inversion of fault–slip data has been applied successfully to areas dominated by transpression (e.g., Burg et al., 2005; Laó-Dávila and Anderson, 2009; De Vicente et al., 2009).

There are some differences between single stress states recorded at individual localities compared to the overall regional stress field. In particular, the σ_1 trend rotates from E–W to NE–SW in the Lanterman Range/Sledgers Glacier area (Fig. 8) where the main faults change strike from NNW–SSE to NW–SE. This could result from a rotation of the sector south of the Sledgers Glacier linked to displacements along younger E–W striking strike–slip systems active in this area post-dating the dominant NNW–SSE left-lateral faults (structural station 8). Alternatively, since the attitude of the main faults follows the orientation of the Ross-related ductile fabric (Fig. 6), the apparent rotation of paleostress field could be explained by the interaction between the regional pre-existing fabric with the far-field stress field. However, were this the case, there should be an increase in the strike–slip component in this southern sector of the study area. Since this is not observed, the second hypothesis appears less feasible.

6.4. Age constrains and regional implications

In northern Victoria Land, the Cenozoic brittle tectonics has been thoroughly investigated by many authors (Salvini et al., 1997; Salvini and Storti, 1999; Rossetti et al., 2000, 2002, 2003; Storti et al., 2001) whereas older brittle structures related to post-Ross Orogeny phases are less well known (Wodzicki and Robert, 1986; Jordan et al., 1984; Capponi et al., 1999). During the present study, we have selected only those faults characterized by a specific type of damage zones and mineralization. Some of these faults are truncated by the Admiralty Intrusives and are hence most likely to be of Paleozoic age. The diffuse veining and hydrothermal alteration associated with these faults is consistent with temperatures in the range 270–320 °C (Crispini et al., 2007c). This suggests that the studied faults were likely active at depths close to the brittle–ductile transition (at least 10 km, Sibson et al., 1988).

The field observations and fault–slip analysis suggests an E–W to NE–SW trending subhorizontal σ_1 for the paleostress tensor, and a sinistrally transpressional tectonic regime. This contrasts markedly with the dextral transtensional NW–SE to NNW–SSE trending strike–slip regime in northern Victoria Land during the Cenozoic (Salvini et al., 1997; Rossetti et al., 2003) with N–S- to NNW–SSE trending σ_1 (Rossetti et al., 2002). We observed clear examples of dextral strike–slip faults overprinting faults related to the sinistral transpressional system described here. Indeed, some of the faults excluded from the stress tensor calculations ("Rest" column of Table 1, especially stops 6, 7 and 10) are consistent with the kinematics of Cenozoic faults reported by Rossetti et al. (2003). This is in agreement with the known longevity of intraplate strike–slip deformation zones, that usually tend to be reactivated many times (Storti et al., 2003). We, therefore, conclude that the studied faults predate the better known Cenozoic structures in this part of Antarctica and that a Paleozoic age is more likely.

The climax of Ross orogenic activity in northern Victoria Land is commonly assigned to the Late Cambrian–Early Ordovician (500–480 Ma), when high-pressure metamorphism occurred (Di Vincenzo et al., 1997), together with voluminous calcalkaline magmatism (Borg et al., 1986 and references therein) and regional deformation (Wright and Dallmeyer, 1991). Less consensus exists concerning the presence of other (younger) Paleozoic tectonic events in the area. Ordovician to Silurian geochronological ages have occasionally been reported in the past (e.g., Adams and Kreuzer, 1984; Dallmeyer and Wright, 1992), including local reactivation of the Lanterman Fault Zone (480–460 Ma; Crispini et al., 2007b) and shear zone development in the inboard Wilson Terrane (about 440 Ma; Di Vincenzo et al., 2007). Lastly, a Devonian event ("Borchgrevink Orogeny") has been suggested by Grindley and Warren (1964) and more recently Capponi et al. (2002) have supplied some radiometric evidence. In the Devonian/Carboniferous, the significance of the Admiralty/Gallipoli magmatic pulse is still widely debated. Despite their clear calcalkaline affinities (Borg et al., 1986), which might suggest a relationship with an accretion/

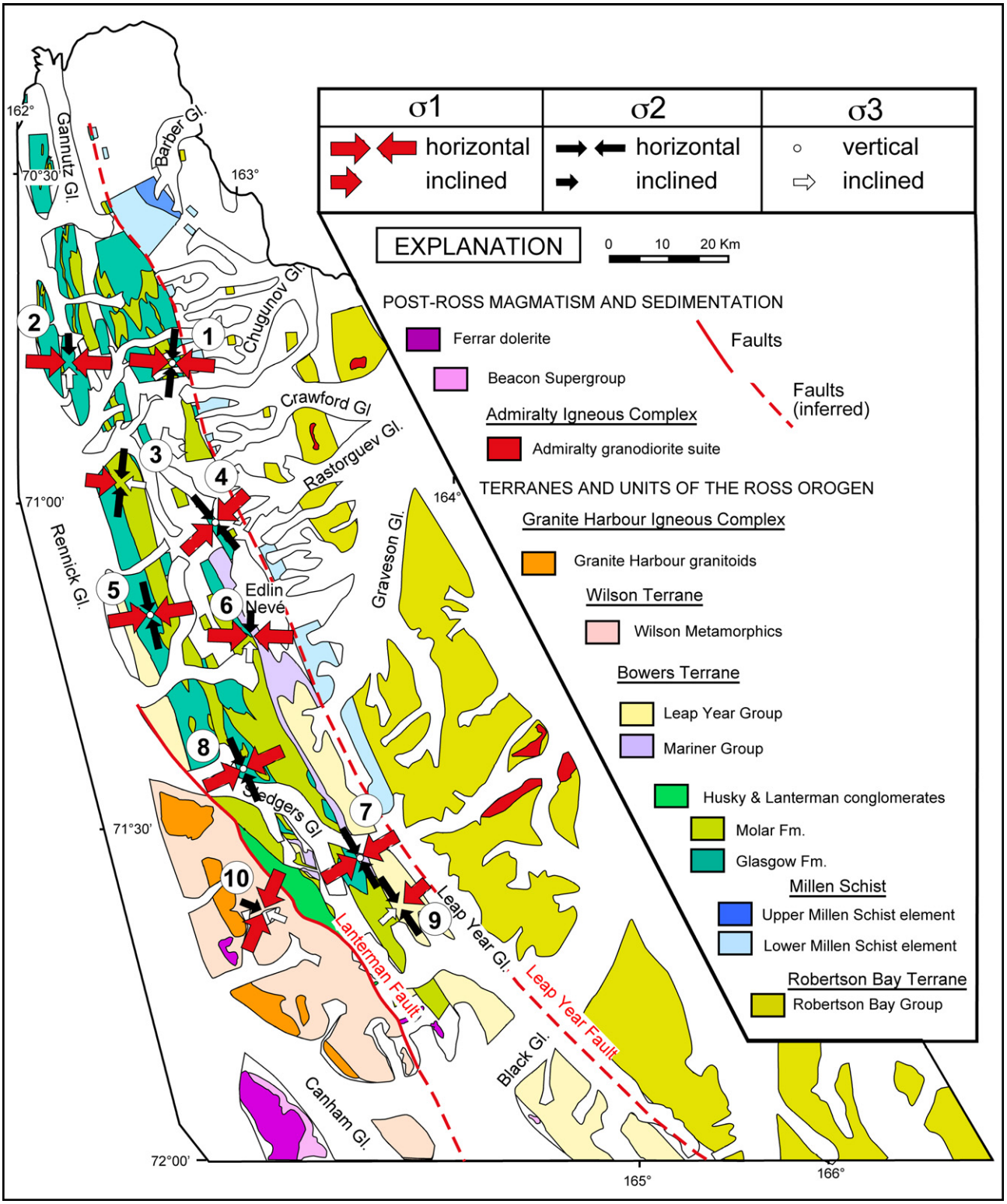

Fig. 8. Geologic map with the trend of the σ_1 axes (red arrows) for the dominant stress field of the study area.

subduction process, no evidence of deformation has so far been described and the plutons seem to be little deformed, shallow crustal, discordant features.

We, therefore, tentatively link the sinistral transpressional deformation either to the waning stages of the Ross Orogeny (Early Ordovician), or to a Late Ordovician–Silurian event still poorly constrained in northern Victoria Land, but more widely recognized in southeastern Australia. Taking into account the former juxtaposition of northern Victoria Land and SE Australia, a Late Ordovician–Silurian deformation phase might be linked to contractional tectonics associated with the early stages (Benambran Orogeny) of the development of the Late Ordovician–Late Devonian Lachlan Fold Belt (e.g., VandenBerg et al., 2000). Significantly, this deformation phase is associated with NE–SW to E–W convergence

(present-day coordinates; Squire and Miller, 2003; Glen et al., 2007). Moreover, structurally controlled mineralizations and veining that formed in the 455–435 Ma interval in the Stawell and Bendigo Zones of SE Australia appear to be generally related to reverse faults (Bierlein et al., 2001, 2004). At Stawell, gold lodes of this age developed during brittle deformation associated with high fluid pressures in a NE–SW and then E–W shortening regime (Miller and Wilson, 2002). The mineralized faults described in northern Victoria Land may have been generated during the same tectonic context (Crispini et al., in press.).

7. Conclusions

In the present study, fault–slip data were inverted to calculate reduced palaeostress tensors through a stepwise procedure that allowed us to compare results obtained from different methods. We found good agreement between FSA and MIM results and a first-order agreement of principal stress axes and *P–B–T* axes calculated by Faultkin. Paleostress inversion methods correctly separated faults of different populations when overprinting relationships had been observed, and in general agree well with field observations, except in cases where fault planes exhibited curved geometries.

We identified a transpressional stress field, that sometimes was represented by two different stress tensors, one purely compressive and one with a wrench component, with a constantly orientated σ_1 axis. This stress field gave rise to steeply-dipping reverse and strike–slip (predominantly sinistral) faults, locally associated with the development of positive flower structures and diffuse veining and hydrothermal alteration in fault zones.

This regional stress field is characterized by an E–W trending, horizontal σ_1 and local rotations into NE–SW directions in the Lanterman Range/Sledgers Glacier area, due either to subsequent block rotation or to the interference between the far-field stresses with pre-existing ductile discontinuities.

This paleostress regime could be linked either to the waning stages of the Ross Orogeny or to a poorly known Ordovician–Silurian tectonic event, that could represent the northern Victoria Land counterpart of the Benambran Orogeny in the Lachlan Fold Belt.

The paleostress regime, overall structural framework and the association with fault-hosted hydrothermal veins constitutes strong similarities with the Stawell and Bendigo Zones of SE Australia, thus suggesting that a Ordovician–Silurian event is the best candidate for the development of such a stress field and related structures. Additional geochronological dating studies are required in order to further test this hypothesis.

Acknowledgments

Fieldwork benefitted from the excellent support of Helicopter NZ; special thanks to Jeff McClintock and Ricky Park.

The Authors thank Blanka Sperner for kindly providing the software FLUMO together with useful suggestions. Richard Allmendinger, Bernard Célérier and Atsushi Yamaji are acknowledged for kindly providing for free the softwares Faultkin and Stereonet, F. S.A. and M.I.M., respectively.

Careful reviews by F. Storti, R. Holdsworth and an anonymous reviewer are greatly appreciated.

This research benefitted from the logistic and financial support of the P.N.R.A. (Programma Nazionale di Ricerche in Antartide).

References

Adams, C., 2006. Style and uplift of Paleozoic terranes in northern Victoria Land, Antarctica: evidence from K–Ar patterns. In: Futterer, K., Damaske, D., Kleinschmidt, G., Miller, H., Tessensohn, F. (Eds.), Antarctica: contributions to Global Earth Sciences. Proceedings of the IX International Symposium of Antarctic Earth Sciences, Potsdam. 8–12/09/2003, 205–213.

Adams, C., Kreuzer, H., 1984. Potassium – argon age studies of slates and phyllites from the Bowers and Robertson Bay terranes, North Victoria Land, Antarctica. Geologisches Jahrbuch B 60, 265–288.

Allmendinger, R.W., Marrett, R.A., Cladouhos, T., 1994. FaultKin V. 4.3.5. A Program for Analyzing Fault–slip Data on a Macintosh Computer. Absoft Corp.. 1988–2004.

Angelier, J., 1979. Determination of the mean principal directions of stresses for a given fault population. Tectonophysics 56 (3–4), T17–T26.

Angelier, J., 1984. Tectonic analysis of fault slip data sets. Journal of Geophysical Research 89, 5835–5848.

Angelier, J., 1990. Inversion of field data in fault tectonics to obtain the regional stress. III. A new rapid direct inversion method by analytical means. Geophysical Journal International 103 (2), 363–376.

Angelier, J., 1994. Fault slip analysis and paleostress reconstruction. In: Hancock, P.L. (Ed.), Continental Deformation. Pergamon Press, Oxford, pp. 53–101.

Angelier, J., Mechler, P., 1977. Sur une méthode graphique de recherche des contraintes principales également utilisable en tectonique et en séismologie: la méthode des dièdres droits. Bulletin de la Société Géologique de France 7 (t. XIX, 6), 1309–1318.

Audemard, F.A., Romero, G., Rendon, H., Cano, V., 2005. Quaternary fault kinematics and stress tensors along the southern Caribbean from fault–slip data and focal mechanism solutions. Earth-Science Reviews 69, 181–233.

Barrett, P.J., 1981. History of the Ross Sea region during the deposition of the Beacon Supergroup 400–180 million years ago. Journal of the Royal Society of New Zealand 11 (4), 447–458.

Bergerat, F., Angelier, J., Andreasson, P.-G., 2007. Evolution of paleostress fields and brittle deformation of the Tornquist Zone in Scania (Sweden) during Permo-Mesozoic and Cenozoic times. Tectonophysics 444, 93–110.

Bierlein, F.P., Christie, A.B., Smith, P.K., 2004. A comparison of orogenic gold mineralisation in central Victoria (AUS), western South Island (NZ) and Nova Scotia (CAN): implications for variations in the endowment of Paleozoic metamorphic terrains. Ore Geology Reviews 25, 125–168.

Bierlein, F.P., Dennis, C.A., Foster, D.A., Reynolds, P., 2001. A geochronological framework for orogenic gold mineralisation in central Victoria, Australia. Mineralium Deposita 36, 741–767.

Borg, S.G., Stump, E., 1987. Paleozoic magmatism and associated tectonic problems of Northern Victoria Land, Antarctica. In: McKenzie, G. (Ed.), Gondwana Six: Structure, Tectonics and Geophysics. American Geophysical Union. Geophysical Monograph, 40, pp. 67–76.

Borg, S.G., Stump, E., Chappel, B.W., McCulloch, E., Stump, E., Wyborn, D., Holloway, J.R., 1984. Compositional polarity of granitoids with implications to regional geology, northern Victoria Land, Antarctica. Geological Society of America 16 (6) Abstracts with Programs.

Borg, S., Stump, E., Holloway, R., 1986. Granitoids of Northern Victoria Land, Antarctica: a reconnaissance study of field relations, petrography, and geochemistry. In: Stump, E. (Ed.), Geological Investigation in Northern Victoria Land. Antarctic Research Series, vol. 46. American Geophysical Union, pp. 115–188.

Bott, M.H.P., 1959. The mechanics of oblique slip faulting. Geological Magazine 96 (2), 109–117.

Burg, J.-P., Célérier, B., Chaudhryc, N.M., Ghazanfarc, M., Gnehma, F., Schnellmann, M., 2005. Fault analysis and paleostress evolution in large strain regions: methodological and geological discussion of the southeastern Himalayan fold-and-thrust belt in Pakistan. Journal of Asian Earth Sciences 24, 445–467.

Bradshaw, J.D., 1987. Terrane boundaries and terrane displacement in northern Victoria Land, Antarctica. Some problems and constraints. In: Leitch, E.C., Scheibner, E. (Eds.), Terrane Accretion and Orogenic Belts. Geodynamics Series, vol. 19. American Geophysical Union, Washington D.C., pp. 199–205.

Bradshaw, J.D., 1989. Terrane boundaries in northern Victoria Land. Memorie Della Società Geologica Italiana 33, 9–15.

Bradshaw, J.D., Begg, J.C., Buggish, W., Brodie, C., Tessensohn, F., Wright, T.O., 1985. New data on Paleozoic stratigraphy and structure in north Victoria Land. New Zealand Antarctic Record 6 (3), 1–6.

Capponi, G., Carosi, R., Meccheri, M., Oggiano, G., 2005. Strain analysis in the Millen Range of Northern Victoria Land, Antarctica. Geologisches Jahrbuch B85, 225–251.

Capponi, G., Castorina, F., Di Pisa, A., Meccheri, M., Petrini, R., Villa, I.M., 2002. The metaigneous rocks of the Barber Glacier area (northern Victoria Land, Antarctica): a clue to the enigmatic Borchgrevink orogeny? In: Gamble, J., Skinner, D., Henrys, S. (Eds.), Antarctica at the Close of a Millennium Royal Society of New Zealand Bulletin, vol. 35, pp. 99–104.

Capponi, G., Crispini, L., Meccheri, M., 1999. Structural history and tectonic evolution of the boundary between the Wilson and Bowers terranes, Lanterman Range, northern Victoria Land, Antarctica. Tectonophysics 312, 249–266.

Cawood, P.A., 2005. Terra Australis Orogen: Rodinia breakup and development of the Pacific and Iapetus margins of Gondwana during the Neoproterozoic and Paleozoic. Earth-Science Reviews 69, 249–279.

Célérier, B., 1988. How much slip on a reactivated fault plane constrain the stress tensor? Tectonics 7 (6), 1257–1278.

Célérier, B., 1999. Fault slip and stress anaylsis (FSA). Available at: <http://www.isteem.univ-mont2.fr/PERSO/celerier/software/fsa.html>.

Collinson, J.W., 1991. The palaeo-Pacific margin as seen from East Antarctica. In: Thomson, M.R.A., Crame, J.A., Thomson, J.W. (Eds.), Geological Evolution of Antarctica. Cambridge University Press, New York, pp. 199–204.

Coulomb, C.A., 1776. Essai sur une application des règles de maximis et de minimis à quelques problèmes de statique relatifs à l'architecture. Mémoires de mathématique & de physique, présentés à l'Académie Royale des Sciences par divers savans 7, 343–382.

Crispini, L., Capponi, G., Federico, L., 2007a. Tectonics at the Bowers – Robertson Bay Terrane boundary, northern Victoria Land (Antarctica). In: Cooper, A.K., Raymond, C.R. (Eds), Antarctica: a Keystone in a changing World. Online Proceedings of the 10th ISAES, USGS Open-File Report 2007-1047, Extended Abstract 073, 4 pp..

Crispini, L., Capponi, G., Federico, L., Talarico, F., 2007c. Gold bearing veining linked to transcrustal fault zones in the Transantarctic Mountains, in Antarctica. In: Cooper, A.K., Raymond, C.R. (Eds), Antarctica: a Keystone in a changing World. Online Proceedings of the 10th ISAES, USGS Open-File Report 2007-1047, Extended Abstract 212, 4 pp..

Crispini, L., Di Vincenzo, G., Palmeri, R., 2007b. Petrology and Ar–Ar dating of shear zones in the Lanterman Range (northern Victoria Land, Antarctica): implications for metamorphic and temporal evolution at terrane boundaries. Mineralogy and Petrology 89 (3–4), 217–249.

Crispini, L., Federico, L., Capponi, G., Talarico, F., The Dorn gold deposit in northern Victoria Land, Antarctica: Structure, hydrothermal alteration, and implications for the Gondwana Pacific margin. In Press, Gondwana Research, Available online 14 April 2010, ISSN 1342-937X, DOI: 10.1016/j.gr.2010.03.010.

Dallmeyer, R.D., Wright, T.O., 1992. Diachronous cleavage development in the Robertson Bay Terrane, Northern Victoria Land, Antarctica: tectonic implications. Tectonics 11 (2), 437–448.

De Paola, N., Holdsworth, R.E., McCaffrey, K.J.W., Barchi, M.R., 2005. Partitioned transtension: an alternative to basin inversion models. Journal of Structural Geology 27, 607–625.

De Vicente, G., Vegas, R., Muñoz-Martín, A., Van Wees, J.D., Casas-Sáinz, A., Sopeña, A., Sánchez-Moya, Y., Arche, A., López-Gómez, J., Olaiz, A., Fernández-Lozano, J., 2009. Oblique strain partitioning and transpression on an inverted rift: the Castilian Branch of the Iberian Chain. Tectonophysics 470, 224–242.

Dewey, J.F., Holdsworth, R.E., Strachan, R.A., 1998. Transpression and transtension zones. In: Holdsworth, R.E., Strachan, R.A., Dewey, J.F. (Eds.), Continental Transpressional and Transtensional Tectonics. Geological Society, London, Special Publications, vol. 135, pp. 1–14.

Diraison, M., Cobbold, P.R., Gapais, D., Rossello, E.A., Le Corre, C., 2000. Cenozoic crustal thickening, wrenching and rifting in the foothills of the southernmost Andes. Tectonophysics 316, 91–119.

Di Vincenzo, G., Carosi, R., Palmeri, R., Tiepolo, M., 2007. A comparative U-Th-Pb (zircon–monazite) and 40Ar–39Ar (muscovite–biotite) study of shear zones in northern Victoria Land (Antarctica): implications for geochronology and localized reworking of the Ross Orogen. Journal of Metamorphic Geology 25, 605–630.

Di Vincenzo, G., Palmeri, R., Talarico, F., Andriessen, P.A.M., Ricci, C.A., 1997. Petrology and geochronology of eclogites from the Lanterman Range, Antarctica. Journal of Petrology 38 (10), 1391–1417.

Dupin, J.-M., Sassi, W., Angelier, J., 1993. Homogeneous stress hypothesis and actual fault slip: a distinct element analysis. Journal of Structural Geology 15 (8), 1033–1043.

Federico, L., Capponi, G., Crispini, L., 2006. The Ross orogeny of the transantarctic mountains: a northern Victoria Land perspective. International Journal of Earth Sciences 95 (5), 759–770.

Ferraccioli, F., Bozzo, E., Capponi, G., 2002. Aeromagnetic and gravity anomaly constraints for an early Paleozoic subduction system of Victoria Land, Antarctica. Geophysical Research Letters 29 (10), 1406–1410.

Fioretti, A.M., Visona, D., Cavazzini, G., Lombardo, B., 1997. Devonian magmatism: implications for the evolution of Northern Victoria Land, Antarctica, and correlation with Southeastern Australia and Northeastern Tasmania. In: Ricci, C. A. (Ed.), The Antarctic Region: Geological Evolution and Processes. Terra Antartica Publications, Siena, pp. 293–296.

Findlay, R.H., Brown, A.V., McClenagham, M.P., 1991. Confirmation of the correlation between Lower Paleozoic rocks in western Tasmania and northern Victoria Land, Antarctica and a revised tectonic interpretation. Memorie Della Società Geologica Italiana 46, 117–133.

Fossen, H., Tikoff, B., 1993. The deformation matrix for simultaneous simple shearing, pure shearing and volume change, and its application to transpression–transtension tectonics. Journal of Structural Geology 15, 413–422.

GANOVEX Team, 1987. Geological map of north Victoria Land, Antarctica, 1:500000-explanatory notes. Geologisches Jahrbuch B66, 7–79.

Glen, R.A., Meffre, S., Scott, R.J., 2007. Benambran Orogeny in the Eastern Lachlan Orogen, Australia. Australian Journal of Earth Sciences 54, 385–415.

Goodge, J.W., 2007. Metamorphism in the Ross orogen and its bearing on Gondwana margin tectonics. In: Cloos, M., Carlson, W.D., Gilbert, M.C., Liou, J.G., Sorensen, S.S. (Eds.), Convergent Margin Terranes and Associated Regions: A Tribute to W.G. Ernst. Geological Society of America, Special Paper, vol. 419, pp. 185–203.

Grindley, G.W., Warren, G., 1964. Stratigraphic nomenclature and correlation in the western Ross Sea region. In: Adie, R.J. (Ed.), Antarctic Geology. North Holland Publ. Comp., Amsterdam, pp. 314–333.

Harland, P.D.W., 1971. Tectonic transpression in Caledonian Spitzbergen. Geological Magazine 108, 27–42.

Holdsworth, R.E., Pinheiro, R.V.L., 2000. The anatomy of shallow-crustal transpressional structures: insights from the Archaean Carajas fault zone, Amazon, Brazil. Journal of Structural Geology 22 (8), 1105–1123. 1.

Holdsworth, R.E., Tavarnelli, E., Clegg, P., Pinheiro, R.V.L., Jones, R.R., McCaffrey, K.J. W., 2002. Domainal deformation patterns and strain partitioning during transpression: an example from Southern Uplands terrane, Scotland. Journal of the Geological Society, London 159, 401–415.

Jordan, H., Findlay, R., Mortimer, G., Schmidt-Thomé, M., Crawford, A., Muller, P., 1984. Geology of the northern Bowers Mountains, North Victoria Land, Antarctica. Geologisches Jahrbuch B60, 57–81.

Kleinschmidt, G., Tessensohn, F., 1987. Early paleozoic westward directed subduction at the Pacific Margin of Antarctica. In: McKenzie, G. (Ed.), Gondwana Six: Structure, Tectonics and Geophysics. American Geophysical Union. Geophysical Monograph, 40, pp. 89–105.

Laird, M.G., 1987. Evolution of the Cambrian-Early Ordovician Bowers Basin, Northern Victoria Land, and its relationship with the adjacent Wilson and Robertson Bay Terranes. Memorie Della Società Geologica Italiana 33, 25–34.

Lamarche, J., Mansy, J.L., Bergerat, F., Averbuch, O., Hakenberg, M., Lewandowski, M., Stupnicka, E., Swidrowska, J., Wajspryc, B., Wieczorek, J., 1999. Variscan tectonics in the Holy Cross Mountains (Poland) and the role of structural inheritance during Alpine tectonics. Tectonophysics 313, 171–186.

Laó-Dávila, D.A., Anderson, T.H., 2009. Kinematic analysis of serpentinite structures and the manifestation of transpression in southwestern Puerto Rico. Journal of Structural Geology 31, 1472–1489.

Liesa, C.L., Lisle, R.J., 2004. Reliability of methods to separate stress tensors from heterogeneous fault–slip data. Journal of Structural Geology 26, 559–572.

Marrett, R., Allmendinger, R.W., 1990. Kinematic analysis of fault–slip data. Journal of Structural Geology 12 (8), 973–986.

Marrett, R., Peacock, D.C.P., 1999. Strain and stress. Journal of Structural Geology 21, 1057–1063.

Matenco, L., Schmid, S., 1999. Exhumation of the Danubian nappes system (South Carpathians) during the Early Tertiary: inferences from kinematic and paleostress analysis at the Getic/Danubian nappes contact. Tectonophysics 314, 401–422.

Merle, O., Gapais, D., 1997. Strains within thrust–wrench zones. Journal of Structural Geology 19 (7), 1011–1014.

Miller, J.Mc.L., Wilson, C.J.L., 2002. The Magdala Lode System, Stawell, southeastern Australia: structural style and relationship to gold mineralisation across the western Lachlan Fold Belt. Economic Geology 97, 325–349.

Pollard, D.D., Saltzer, S.D., Rubin, A.M., 1993. Stress inversion methods: are they based on faulty assumptions? Journal of Structural Geology 15 (8), 1045–1054.

Ramsay, J.G., 1980. The crack–seal mechanism of rock deformation. Nature 284, 135–139.

Ramsay, J.G., Lisle, R.J., 2000. The techniques of modern structural geology. In: Applications of Continuum Mechanics in Structural Geology, vol. 3. Academic Press, London.

Ricci, C.A., Talarico, F., Palmeri, R., 1997. Tectonothermal evolution of the antarctic paleo-pacific margin of Gondwana: a Northern Victoria Land perspective. In: Ricci, C.A. (Ed.), The Antarctic Region: Geological Evolution and Processes. Terra Antarctica Publication, Siena, pp. 293–296.

Robin, P.-Y., Cruden, A.R., 1994. Strain and vorticity patterns in ideally ductile transpression zones. Journal of Structural Geology 16, 447–466.

Rocchi, S., Capponi, G., Crispini, L., Di Vincenzo, G., Ghezzo, C., Meccheri, M., Palmeri, R., 2003. Mafic rocks at the Wilson–Bowers terrane boundary and within the Bowers Terrane: clues to the Ross geodynamics in northern Victoria Land, Antarctica. Abstract of the 9th International Symposium on Antarctic Earth Sciences, September 8–12, Potsdam, Germany.

Rossetti, F., Lisker, F., Storti, F., Laufer, A.L., 2003. Tectonic and denudation history of the Rennick Graben (North Victoria Land): implications for the evolution of rifting between East and West Antarctica. Tectonics 22 (2), 1016–1034.

Rossetti, F., Storti, F., Laufer, A.L., 2002. Brittle architecture of the Lanterman Fault and its impact on the final terrane assembly in North Victoria Land, Antarctica. Journal of the Geological Society of London 159 (2), 159–173.

Rossetti, F., Storti, F., Salvini, F., 2000. Cenozoic noncoaxial transtension along the western shoulder of the Ross Sea, Antartica, and the emplacement of McMurdo dyke arrays. Terra Nova 12, 60–66.

Saintot, A., Angelier, J., 2002. Tectonic paleostress fields and structural evolution of the NW-Caucasus fold-and-thrust belt from Late Cretaceous to Quaternary. Tectonophysics 357, 1–31.

Salvini, F., Brancolini, G., Busetti, M., Storti, F., Mazzarini, F., Coren, F., 1997. Cenozoic geodynamics of the Ross Sea region, Antarctica: crustal extension, intraplate strike-slip faulting, and tectonic inheritance. Journal of Geophysical Research 102 (B11), 24669–24696.

Salvini, F., Storti, F., 1999. Cenozoic tectonic lineaments of the Terra Nova Bay region, Ross Embayment, Antarctica. Global and Planetary Change 23, 129–144.

Sanderson, D.J., Marchini, W.R.D., 1984. Transpression. Journal of Structural Geology 6, 449–458.

Scheidegger, A.E., 1964. The tectonic stress and tectonic motion direction in Europe and Western Asia as calculated from earthquake fault plane solutions. Bulletin of the Seismological Society of America 54, 1519–1528.

Sibson, R.H., Robert, F., Poulsen, K.H., 1988. High-angle reverse faults, fluid-pressure cycling, and mesothermal gold–quartz deposits. Geology 16, 551–555.

Sippel, J., Scheck-Wenderoth, M., Reicherter, K., Mazur, S., 2009. Paleostress states at the south-western margin of the Central European Basin System – application of fault–slip analysis to unravel a polyphase deformation pattern. Tectonophysics 470 (1–2), 129–146.

Sperner, B., Ratschbacher, L., Ott, R., 1993. Fault-striae analysis: a turbo-pascal program package for graphical presentation and reduced stress tensor calculation. Computers & Geosciences 19 (9), 1361–1388.
Squire, R.J., Miller, J.Mc.L., 2003. Synchronous compression and extension in East Gondwana: tectonic controls on world-class gold deposits at 440 Ma. Geology 31 (12), 1073–1076.
Storti, F., Holdsworth, R.E., Salvini, F., 2003. Intraplate strike-slip deformation belts. In: Storti, F., Holdsworth, R.E., Salvini, F. (Eds.), Intraplate Strike-slip Deformation Belts. Geological Society London, Special Publication, vol. 210, pp. 1–14.
Storti, F., Rossetti, F., Salvini, F., 2001. Structural architecture and displacement accommodation mechanisms at the termination of the Priestley Fault, northern Victoria Land, Antarctica. Tectonophysics 341, 141–161.
Stump, E., 1995. The Ross Orogen of the Transantarctic Mountains. Cambridge University Press.
Tavarnelli, E., Holdsworth, R.E., Clegg, P., Jones, R.R., McCaffrey, K.J.W., 2004. The anatomy and evolution of a transpressional imbricate zone: Southern Uplands, Scotland. Journal of Structural Geology 26, 1341–1360.
Tchalenko, J., Ambraseys, N.N., 1970. Structural analysis of the Dasht-e Bayaz (Iran) earthquake fractures. Geological Society of America Bulletin 81, 41–60.
Twiss, R.J., Unruh, J.R., 1998. Analysis of fault slip inversions; do they constrain stress or strain rate? Journal of Geophysical Research, B, Solid Earth and Planets 103 (6), 12,205–112,222.
VandenBerg, A.H.M., Willman, C.E., Maher, S., Simons, B.A., Cayley, R.A., Taylor, D.H., Morand, V.J., Moore, D.H., Radojkovic, A., 2000. The Tasman Fold Belt System in Victoria. Geological Survey of Victoria Special Publication.
Vaughan, A.P.M., Pankhurst, R.J., 2008. Tectonic overview of the West Gondwana margin. Gondwana Research 13 (2), 150–162.
Veevers, J.J., 2000. Billion-year Earth History of Australia and Neighbours in Gondwanaland. In: Veevers, J.J. (Ed.). GEMOC Press, Sydney.
Wallace, R.E., 1951. Geometry of shearing stress and relation to faulting. Journal of Geology 59 (2), 118–130.
Wang, X., Neubauer, F., 1998. Orogen-parallel strike-slip faults bordering metamorphic core complexes: the Salzach–Enns fault zone in the Eastern Alps, Austria. Journal of Structural Geology 20 (6), 799–818.
Weaver, S.D., Bradshaw, J.D., Laird, M.G., 1984. Geochemistry of Cambrian volcanics of the Bowers Supergroup and implications for the Early Paleozoic tectonic evolution of northern Victoria Land, Antarctica. Earth and Planetary Science Letters 68, 128–140.
Woodcock, N.H., Mort, K., 2008. Classification of fault breccias and related fault rocks. Geological Magazine 145, 435–440.
Wright, T.O., Dallmeyer, R.D., 1991. The age of cleavage development in the Ross orogen, northern Victoria Land, Antarctica: evidence from Ar/Ar whole rock slate ages. Journal of Structural Geology 13, 677–690.
Wright, T.O., Ross, R.J., Repetski, J.E., 1984. Newly discovered youngest Cambrian or oldest Ordovician fossils from the Robertson Bay terrane (formerly Precambrian), Northern Victoria Land, Antarctica. Geology 12, 301–305.
Wodzicki, A., Robert, R., 1986. Geology of the Bowers Supergroup, central Bowers Mountains, northern Victoria Land. In: Stump, E. (Ed.), Geological Investigation in Northern Victoria Land. Antarctic Research Series, vol. 46. American Geophysical Union, pp. 39–68.
Yamaji, A., 2000. The multiple inverse method; a new technique to separate stresses from heterogeneous fault–slip data. Journal of Structural Geology 22 (4), 441–452.
Yamaji, A., Sato, K., 2005. MI Viewer, Version 4.10. Division of Earth and Planetary Sciences. Kyoto University, Kyoto.
Yamaji, A., Sato, K., Otsubo, M., 2005a. Multiple Inversion Method Main Processor, Version 5.31. Division of Earth and Planetary Sciences, Kyoto University, Kyoto.
Yamaji, A., Sato, K., Otsubo, M., 2005b. Multiple Inversion Method Software Package — User's Guide. Division of Earth and Planetary Sciences, Kyoto University, Kyoto.
Zalohar, J., Vrabec, M., 2007. Paleostress analysis of heterogeneous fault–slip data: the Gauss method. Journal of Structural Geology 29, 1798–1810.